This is a preprint (submitted) version of the final VoR Conference Paper published in:
Characterisation and Engineering Properties of Natural Soils Volume 3-4, Pages 2289 - 2327
2007 1st International Workshop on Characterisation and Engineering Properties of Natural Soils

Geotechnical characterization and properties of Venice lagoon heterogeneous silts

P. Simonini, G. Ricceri & S. Cola
Department of Hydraulic, Maritime, Environmental and Geotechnical Engineering (IMAGE)
University of Padova, Padova, Italy

ABSTRACT: To protect the city of Venice against recurrent flooding, a huge project has been undertaken involving the design and construction of movable gates located at the three lagoon inlets for controlling tidal flow. The design of the gate foundations demands accurate geotechnical characterization of the Venice lagoon soils, composed of a predominantly silt fraction combined with clay and/or sand forming an erratic interbedding of various sediments, whose basic mineralogical characteristics vary narrowly. To this end, two typical test sites in the lagoon - the *Malamocco Test Site* and the *Treporti Test Site* – were selected for the mechanical soil characterization and for a site-specifically calibration of the most widely used geotechnical investigation tools. Besides a presentation of the main geological features of the lagoon sediments, the paper presents and discusses the main outcome of the research carried out at the *Malamocco Test Site* and some results from the *Treporti Test Site*.

1 INTRODUCTION

The worldwide-known historic city of Venice continues to preserve a rather precarious equilibrium with the surrounding lagoon, although the margin of security is being eroded at an ever increasing rate. The rate of environmental deterioration is being accelerated by the increasing frequency of the flooding of the historic city – referred as to '*acqua alta*' (i.e. literally '*high water*') - caused by the natural eustatic rise of the sea level, by natural subsidence and by a regional man-induced subsidence, the latter particularly important between 1946 and 1970 (Butterfield et al. 2003). Figure 1 shows the Venice lagoon in the present configuration: through the inlets of Malamocco, Lido and Chioggia flows the tide, becoming, under particular atmospheric conditions, *acqua alta*, that means flooding of the historic city.

The first comprehensive geotechnical and geological studies on Venice lagoon soils were carried out between 1965 and 1975. Mineralogical and paleontological studies on sediments from the site Motte di Volpego (Figure 1) were performed by Bonatti (1968). In 1970 the Italian Government through the Consiglio Nazionale delle Ricerche (CNR) commissioned a 1000 m deep borehole, located at Tronchetto (Figure 1) to estimate the aquifer and aquitard system and the geotechnical properties relevant to an evaluation of the subsidence problem (Favero et al. 1973; Rowe 1973; Ricceri & Butterfield 1974).

Between 1970s and 1980s, the shallowest ground of the lagoon has been extensively studied, but only through standard geotechnical investigations necessary for the design of the foundations of new large industrial settlemements on the mainland.

Relevant information on the mechanical behaviour of lagoon clayey/silty materials sampled at Fusina (Figure 1), a small village facing to the inner lagoon where a thermoelectric power plant is located, was also provided by Cola (1994).

To protect the city of Venice and the surrounding lagoon against the recurrent flooding, a huge project was undertaken at the beginning of the '80s under the directive of Italian

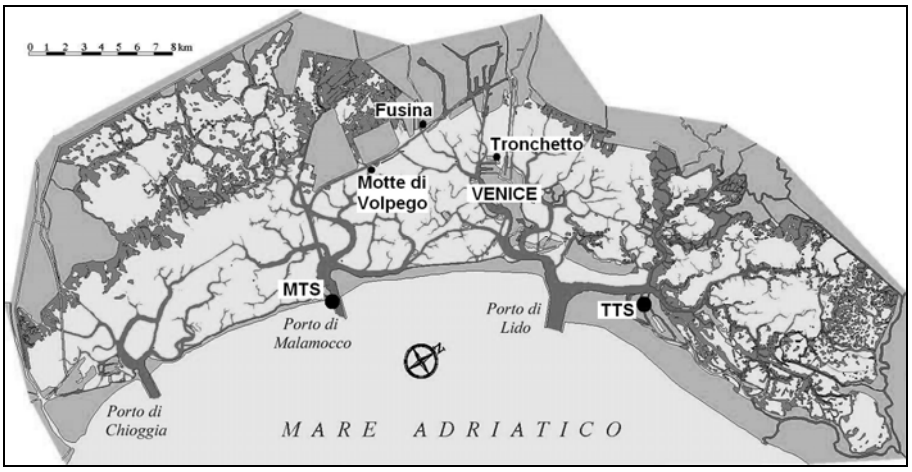

Figure 1. View of the Venice lagoon with the locations of test sites.

Government, involving the design and construction of movable gates located at the three lagoon inlets (Gentilomo 1997). These gates, controlling the tidal flow, temporarily separate the lagoon from the sea at the occurrence of particularly high tides, whose annual frequency is continuously increasing (Harleman et al. 2000).

Therefore, comprehensive geotechnical studies were necessarily carried out to characterize the Venetian soils at the inlets to achieve a suitable design of the movable gates foundations. Preliminary standard geotechnical investigations were therefore performed in the late 1980s, to draw relevant soil profiles along with cross sections of the three lagoon inlets and to estimate significant geotechnical properties for a preliminary selection of gate foundations.

From the geological and geotechnical investigations carried out so far, it turned out that the main characteristic of the lagoon soils is the presence of a predominant silt fraction, combined with clay and/or sand. These form a chaotic interbedding of different sediments, whose basic mineralogical characteristics vary narrowly, as a result of similar geological origins and common depositional environment. This latter feature, together with the relevant heterogeneity of soil layering, suggested to concentrate the researches on some selected test sites, considered as representative of typical soil profiles, where relevant in-situ and laboratory investigations could be carried out for a careful characterization of the Venetian lagoon soils.

The first test site, namely the *Malamocco Test Site* (MTS) (Cola & Simonini 1999, 2002) was located at the Malamocco inlet (Figure 1). Within a limited area, a series of investigations that included boreholes, piezocone (CPTU), dilatometer (DMT), self-boring pressuremeter (SBPM) and cross hole tests (CHT) were performed on contiguous verticals. In addition a continuous borehole was carried out for a very careful soil mineralogical classification.

One of the main aims of the MTS was to evaluate the reliability of the most widely used charts or correlative equations for the piezocone and dilatometer interpretation on the basis of the comparison with the results of the laboratory tests, with the aim of characterizing soil profile and the main geotechnical properties in an economical way (Simonini & Cola 2000; Ricceri et al. 2002). Due to the influence of high soil heterogeneity, relevant difficulties were however encountered in comparing the relevant soil properties with those directly estimated from site tests. The absence of any clear horizontal layering provided no absolute certainty in carrying out a comparison of material properties exactly within the same type of soil.

The comprehensive laboratory test program completed at MTS (Cola & Simonini 2002; Biscontin et al. 2001, 2006) emphasized the very heterogeneous nature of the Venice soils: in order to define even the simplest properties with a certain degree of accuracy, a relatively large number of tests was necessarily required. In addition, due to the high silty content and the low-structured nature, the sediments are extremely sensitive to stress relief and disturbance due to sampling, thus affecting a careful the stress history evaluation and a satisfactory stress-strain-time mechanical characterization.

A new test site was therefore selected, namely the *Treporti Test Site* (TTS) (Simonini 2004), which is located at the inner border of the lagoon, very close to the inlet of Lido (Figure 1). The goal of TTS was to measure directly in-situ the stress-strain-time properties of the

heterogeneous Venetian soils. At the TTS a vertically-walled circular embankment, loading up the ground to slightly above 100 kPa, was very recently constructed, measuring, along with and after the construction, the relevant ground displacements together with the pore pressure evolution. To this end, the ground beneath the embankment was heavily instrumented using plate extensometer, differential micrometers, GPS, inclinometers, piezometers and load cells. Boreholes with undisturbed sampling, traditional CPTU (Gottardi & Tonni 2004) and DMT (Marchetti et al. 2004), seismic SCPTU and SDMT (Mayne & McGillivray 2004) were employed to characterize soil profile and estimate the soil properties for comparison with those directly measured in situ.

Besides the presentation of some geological features of the lagoon sediments, the paper collects and discusses the main results concerning the characterization of the Venice lagoon heterogeneous sandy and clayey silts based on field and laboratory tests carried out mostly at MTS and TTS.

2 GEOLOGICAL DESCRIPTION OF THE VENICE LAGOON

2.1 *Geological and recent history*

The Northern Italian lowlands, namely the Padana and Veneta plains, were formed through the fluvial transport of sediments coming from the erosion of the surrounding Alps and Apennines.

At the end of the Pliocene epoch, the sea level was much higher than today and the Padana and Veneta plains were submerged.

The Pleistocene epoch was characterized by several glaciation and interglaciation periods with alternating regression and transgression of the shoreline. At the apex of last Würmian (Wiscontsinian) glaciation, the shoreline was located around two hundred kilometres from the present position and, therefore, the Padana and Veneta plains together with a part of the Northern Adriatic Sea were emerged.

Then, a warmer period set in about 15,000 years ago and the sea level rose during the de-glaciation period, reaching, between 7000 and 5000 years ago, a value slightly higher than the present one. The origin of the Venice lagoon is traced around 6000 year ago, during the flandrian transgression, with the sea water diffusing into a pre-existing lacustrine basin.

In the Venetian lagoon, the upper hundred metres below mean sea level (MSL) are characterized by a complex system of sands, silts and silty clays chaotically accumulated during the Würmian glaciations (Favero et al. 1973). The Holocene epoch is responsible only for the shallowest lagoon deposits, up to 10-15 m below ground level.

The top layer of Würmian deposits is composed of a crust of highly overconsolidated very silty clay, commonly referred as to *caranto,* on which many historical Venetian buildings are founded through driven wooden piles. It was subject to a process of overconsolidation as a result of exsiccation during the 10,000 year emergence of the last Pleistocenic glaciation. Moving from the mainland towards the shoreline, the *caranto* layer lies at depths increasing from less then 5 m to about 16 m below MSL (Gatto & Previatello 1974).

The present lagoon morphology is the consequence of the intensive human action and of the recent environmental damages. In fact, since the first Venetian citizens settled on the islands (around XII century), the main engineering activities concerned with the conservation of efficient communications between lagoon and sea and the preservation of the city insularity (Colombo 1986). More particularly, to avoid lagoon filling the Venetians diverted the rivers Brenta, Sile, Piave into extensive canals around the lagoon periphery and constructed robust stone-walls to protect the channel and island banks against erosion. The shape of the three lagoon inlets has been also continuously modified: after the second world war, the sea bottom at the Malamocco inlet was very deeply dredged to allow the large oil tankers to reach the Venice / Marghera port through the so called "*oil canal*". All these modifications caused a continuous decrease of sediment balance, with a significant reduction of the area covered by marshes and wetlands. Figures 2*a,b* show a comparison between the lagoon morphology in the XII century with that of the XX century.

To appreciate the high level of interbedding and interdigitation characterizing the youngest soils up to 50-60 m of depth, soil profiles from Fusina, Motte di Volpego, Tronchetto, Malamocco and Treporti are sketched in Figure 3. Note that the majority of soils belong to

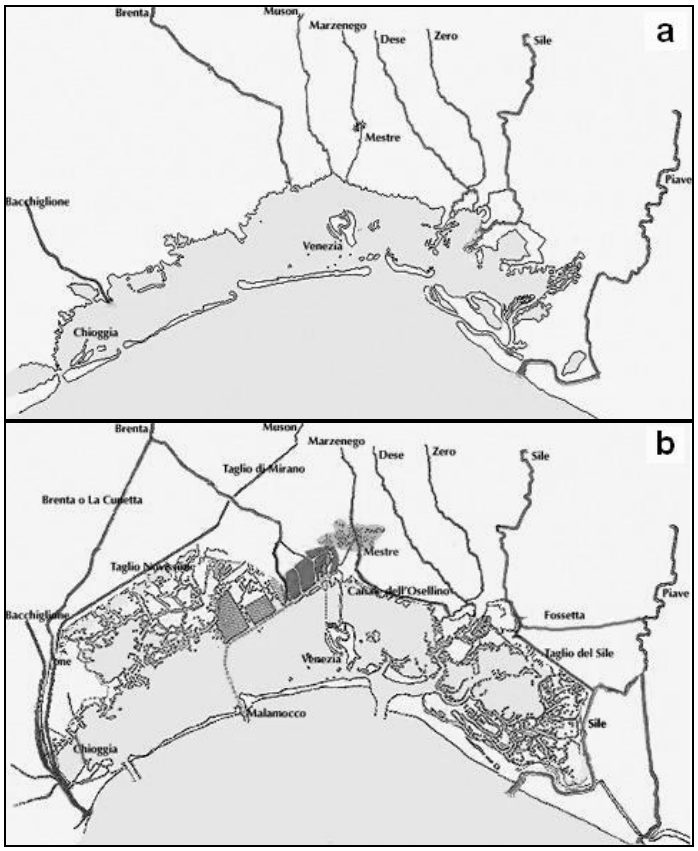

Figure 2. Morphology of the Venice lagoon: 700 years ago (*a*) and at present (*b*).

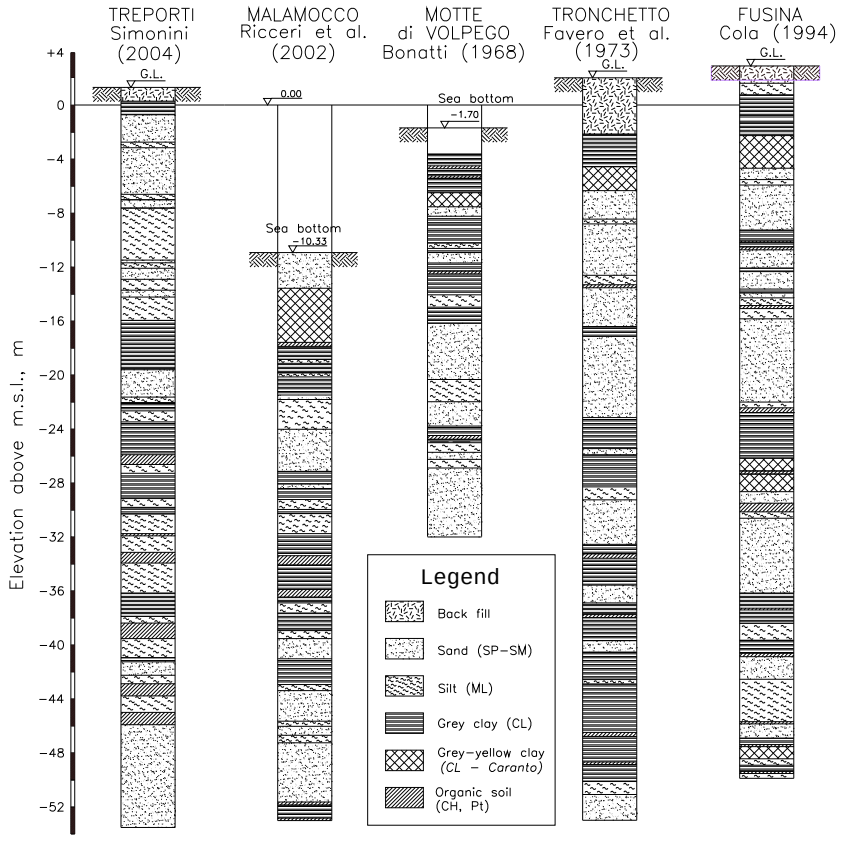

Figure 3. Typical soil profiles of the Venice lagoon.

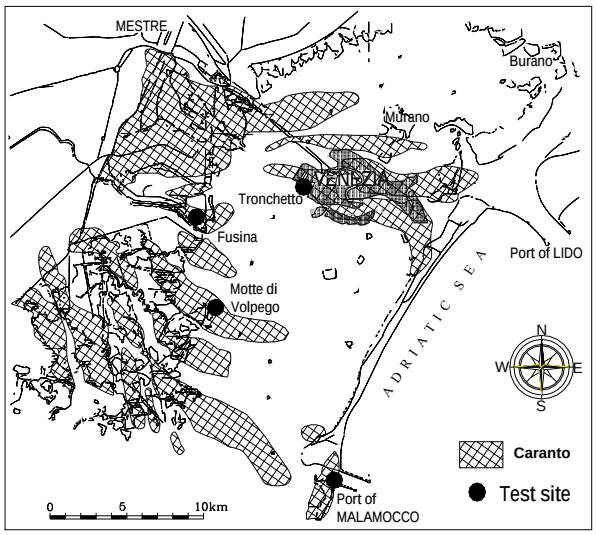

Figure 4. Map of *caranto* in the central part of the lagoon (from Gatto and Previatello 1974).

sands, silts and silty clays with the presence of several layers of peat: the high heterogeneity is clearly evident at larger scale, but significant material variation may be observed even at centimetre scale. Mineralogical and paleontological studies of cores, carried out up to 50-60 m below MSL at Motte di Volpego (Bonatti 1968), Tronchetto (Favero et al. 1973), Malamocco (Curzi 1995) and, more recently at the Lido inlet (Dip. Scienze della Terra di Ferrara et al. 2004), detected five depositional units.

The shallowest Holocene unit is mainly composed by marine sands with significant shell content along with the shoreline and by finer sediments with significant organic matter in the inner part of the lagoon. The underlying units are mainly formed by fluviatile sediments organized in fining-upward structures, sometimes eroded or lightly desiccated at the top, due to a temporary regression of the shoreline or to brief emersion periods. The thin peaty layers should be related to the occasional presence of lacustrine environment. The rate of accumulation is relatively high, about 3 mm/year in average.

In each profile the *caranto* is easily recognizable for the typical grey-yellow colour and the presence of numerous fissures with oxidation traces. The *caranto* layer, slightly sloping toward the shoreline, has thickness varying from a few of centimetres up to some metres. Figure 4 (from Gatto & Previatello 1974) shows a reconstruction of the *caranto* plan distribution based on data coming from different sites in the lagoon: to note that the *caranto*, locally eroded by rivers during the Würmian emergence, covers a great part of the lagoon area.

2.2 *Characteristics of the sediments and porewater pH*

To determine the mineralogical composition of Venetian sediments, samples from MTS were analysed by X-ray diffractometric technique (Curzi 1995). Particularly three analyses were performed: on the bulk samples, on the sand fraction and on the clay fraction, the latter being separated through sedimentation in water and then treated with HCl. Figure 5 depicts the profile of the mineralogical composition obtained from the three analyses, while Table 1 summaries the overall composition: note that the carbonates, mainly a mixture of detrital calcite and dolomite crystals, are generally the most abundant component. Quartz, feldspar, muscovite (2M micas) and chlorite are other significant components.

Sandy soils show two distinct types of petrographic sources, namely the *granitic* or *Padana* province and the *limestone-dolomite* or *Veneta* province. The first one, characterized by a siliceous-clastic composition, is due to sediments from the basins of the Po and Adige rivers whereas the second one, showing prevalently carbonate sediments (with dolomite more abundant than calcite), is shared among the basins of Brenta, Piave, Livenza and Tagliamento rivers. The *Padana* and *Veneta* contributions are mixed together, the first one prevailing at higher depths (Favero et al. 1973).

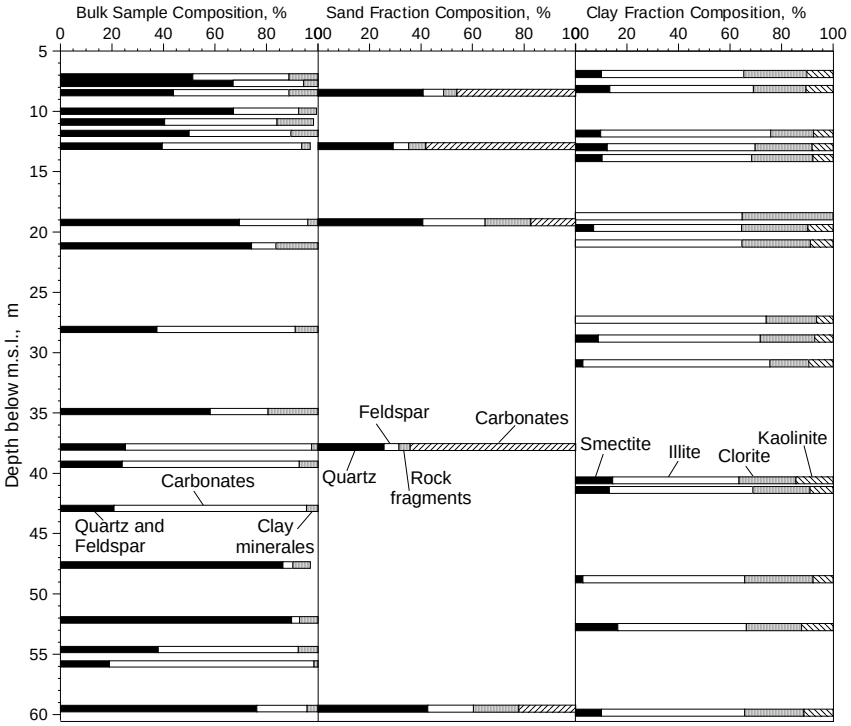

Figure 5. Mineralogical composition for bulk samples, sand fraction and clay fraction of the sediments from the MTS.

Table 1. Major components of some samples from MTS (X Ray-diffractometric analysis).

Sample depth (m)	Calcite & Dolomite (%)	Quartz (%)	Feldspar (%)	Muscovite (%)	Chlorite & Kaolinite (%)	Chlorite/ Smectite (%)	Illite/ Smectite (%)
7.14	37.2	35.7	15.8	6.3	5.0		
7.67	27.4	45.0	22.0	3.8	1.8		
8.45	44.7	40.5	3.4	5.7	3.7	2.0	
9.98	25.3	47.0	20.2	4.5	2.4		
10.88	43.6	26.3	14.2	8.6	5.6		
11.83	39.5	34.6	15.4	7.6	2.9		
12.88	54.1	23.1	16.4	1.7	1.5		
19.20	26.5	25.7	43.8	2.0	2.0		
21.15	9.5	42.3	31.8	11.2	4.6		0.6
28.08	53.6	28.6	8.9	4.5	4.2		
34.88	22.4	33.6	24.6	14.0	5.4		
37.82	72.2	16.5	8.7	1.3	1.3		
39.25	68.7	21.6	2.4	4.5	2.8		
42.90	74.6	17.8	3.1	2.9	1.6		
47.60	4.0	43.3	43.0	4.3	2.4		
52.14	3.1	50.5	39.3	4.5	2.6		
54.61	54.4	29.1	8.9	4.9	2.7		
55.80	79.3	16.2	2.9	0.8	0.8		
59.51	19.5	66.3	9.9	1.1	2.2		1.0

Sands appear immature, with a mean rounding index, evaluated in accordance with Powers' scale (Powers 1953), ranging between 0.23 and 0.34. Typical grain shapes of sand and silt are shown in Figures 6*a*,*b*: quartz and feldspars grains are generally angular, suggesting they were not transported for any extended length of time. Similar conclusions may be drawn by the fact that feldspars and micas are generally relatively fresh with extensive alteration appearing

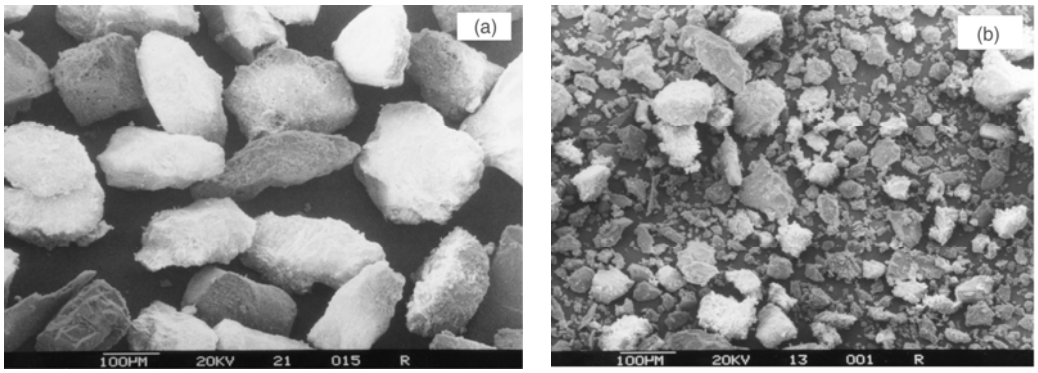

Figure 6. Electromicroscope photos for granular soils from MTS: *a*) sand, *b*) silt (Cola and Simonini, 2002).

occasionally on crystal surfaces.

Along with the variation of the grain-size distribution from sands to clays, the carbonate and quartz-feldspar fractions decrease when the content in clay minerals increases.

As shown in the third column of Figure 5, the composition of the carbonate-free clay fraction seems to be rather homogenous at various levels: clay minerals, not exceeding 20% of total weight, are mainly composed of illite (50-60%) with chlorite, kaolinite and smectites as secondary minerals. X-ray diffractometer traces indicated that small amounts of quartz and feldspar are also present in the clay fraction.

Illite, kaolinite and chlorite appear generally highly crystallized, suggesting a detrital origin. Small amounts of smectites and interstratified illite-smectite minerals, due to chemical alteration occurred in the depositional environment, are occasionally present.

Figures 7*a,b* depict electromicroscope photos taken on undisturbed silty clay samples collected at Fusina at depths of 4.4 m and 12.3 m respectively (Cola 1994). The upper sample of Holocene epoch is characterized by particle packets connected in a relatively continuous and regular assemblage with an alveolar structure, probably due to a low energy lagoon environment. In the lower sample, the particles seem to be aggregated with an irregular structure in small, well-defined packets and arranged by edge-to-face or edge-to-edge contacts, characteristic of a higher energy depositional environment. This latter feature is in accordance with the observations of Bonatti (1968) who noted, in samples collected at Motte di Volpego (below 10 m from GL), chaotic structures and micro-cross stratification, these being characteristic features of sediments deposited from turbulent, rapidly moving masses of water such as rivers.

Comparing in Figure 8*a* the $CaCO_3$ profiles determined at Motte di Volpego, Tronchetto, MTS and TTS, it can be noticed that the carbonates (Calcite and Dolomite) are almost the major component, with percentages exceeding of 50-70% with the exception of an about 3-5 m thick layer with reduced $CaCO_3$ concentration, at depth varying between 20 and 27 m below MSW. Some other low-carbonate episodes exist both at higher and smaller depths, especially at MTS.

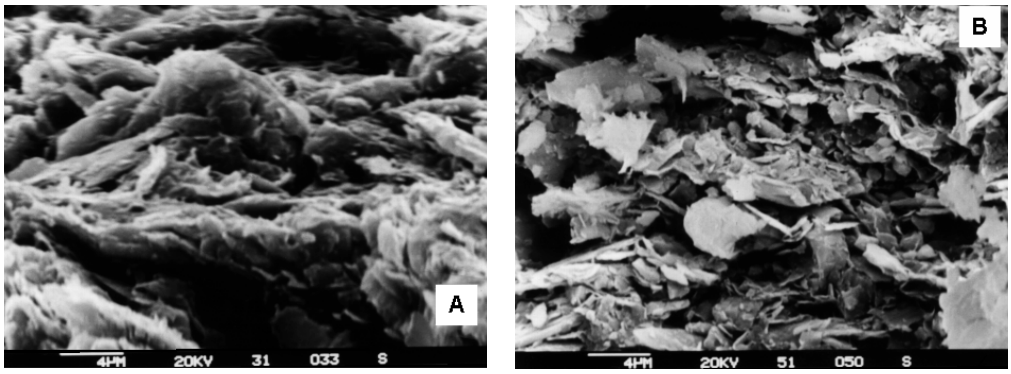

Figure 7. Electromicroscope photos for cohesive soils from Fusina (Cola 1994): *a*) sample at 4.4 m of depth; *b*) sample at 12.3 m of depth.

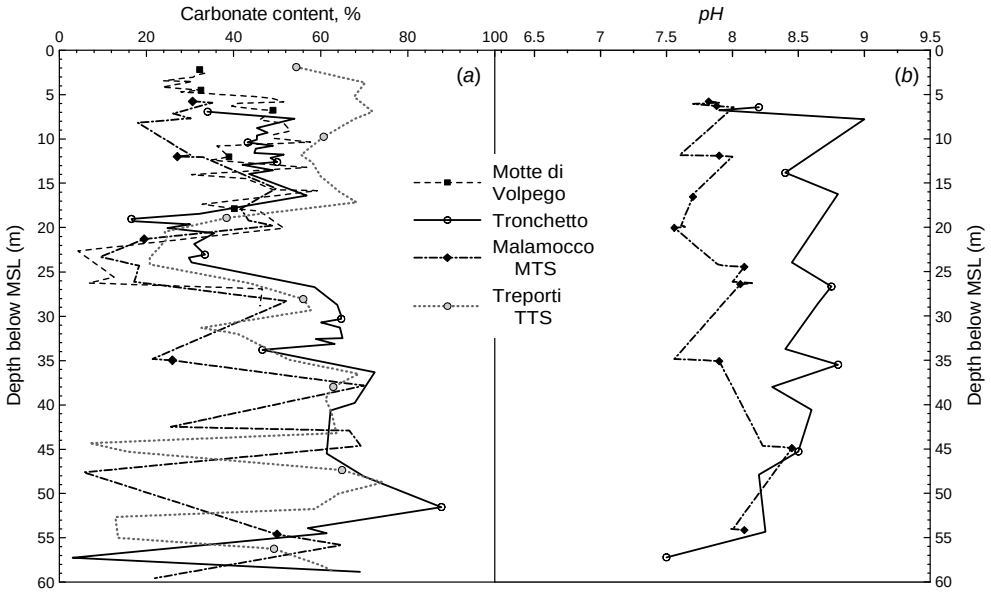

Figure 8. (a) Carbonate profiles at Motte di Volpego, Tronchetto, MTS and TTS; (b) *pH* profiles at Trochetto and MTS.

The reductions of $CaCO_3$ together with the presence of peat or organic soils - relatively common in the lagoon area - could be attributed to lacustrine sedimentation episodes.

Profiles of *pH* measured at Tronchetto and MTS are depicted in Figure 8*b*. Slightly lower values were recorded at MTS, especially at intermediate depths. Oscillation of *pH* at both sites can be noted, with the higher values probably related to low $CaCO_3$ content, being the presence of the carbonatic environment a neutralizer of water acidity.

2.3 *Heterogeneity*

In order to check the soil heterogeneity, TAC scanning was carried out on some MTS samples.

Figure 9*a* shows the density profile in Hounsfield units (HU) obtained using medical TAC equipment of a typical sample taken at 21.7 m below MSL. To convert the measured HU density into kN/m^3 unit the correlation:

$$\gamma\ (\mathrm{kN/m^3}) = \gamma[(\mathrm{HU})+1016.3]/110.9 \qquad (1)$$

proposed by Cortellazzo et al. (1995) for some North-Italian soils, was used.

Figure 9*b* reports the TAC density profile converted in SI units together with the in-situ void ratio e_0, the latter determined at 10 mm-spaced intervals. Both quantities give a relatively irregular trend along the specimen without showing any particular coincidence between the two profiles and with variations around 10-15% of the average value.

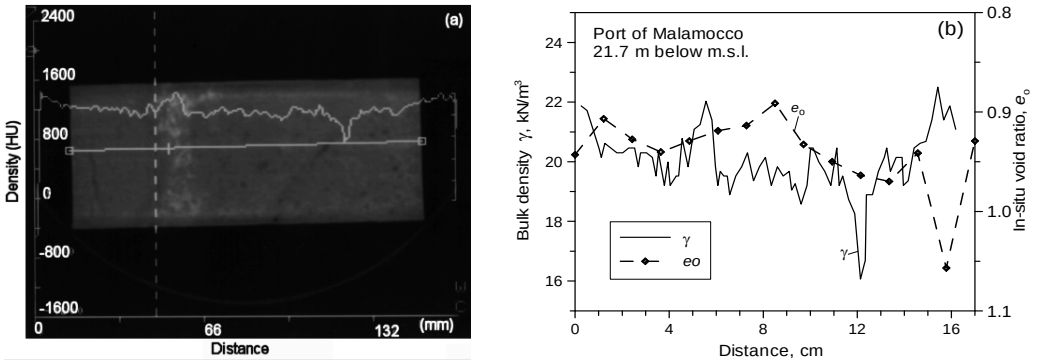

Figure 9. TAC analysis on a sample at 21.7m of depth below MSL in MTS: (*a*) photo and density in HU units, (*b*) density in geotechnical units and void ratio.

3 THE MALAMOCCO TEST SITE

3.1 *Soil profile and basic properties*

In order to reconstruct the detailed profile of soil at MTS, continuous coring was performed along two contiguous verticals using double piston samplers, a standard 10 cm diameter sampler and a larger one with diameter of 20 cm. Freezing technique was used in sandy layers.

Figure 10 shows the basic soil properties as a function of depth. For classification purposes the Venetian soil classes have been reduced to three: medium to fine sand (SP-SM), silt (ML) and very silty clay (CL). Features to note are:

- The predominance of silty and sandy fraction can be clearly appreciated: the three soil classes occur approximately in proportions of 35% SM-SP, 20% ML, 40% CL and 5% medium plasticity clays and organic soils (CH, OH and Pt). Percentages of silt exceeding 50% are present in 65% of samples analyzed;
- Sands are relatively uniform but moving towards finer materials the soils become more graded: the coarser the materials, the lower the coefficient of non-uniformity U, whose range increases with the decreasing mean particle diameter D_{50}.
- Atterberg limits are characterized by average values of liquid limit LL = 36±9% and of plasticity index PI = 14±7%. Activity A=PI/CF (CF=clay fraction) is low, the great majority of samples falling in the range 0.25<A<0.50.
- Significant variations have been observed in saturated unit weight γ_{sat}, even in cores a few centimeters long (specific gravity G_S = 2.77±0.03);
- Void ratio e_o lies in the range between 0.7 and 1.0 from 19 m to 36 m below m.s.l.; at greater depths, it is lower and falls in the range 0.6-0.75 (higher values are due to laminations of organic soils).

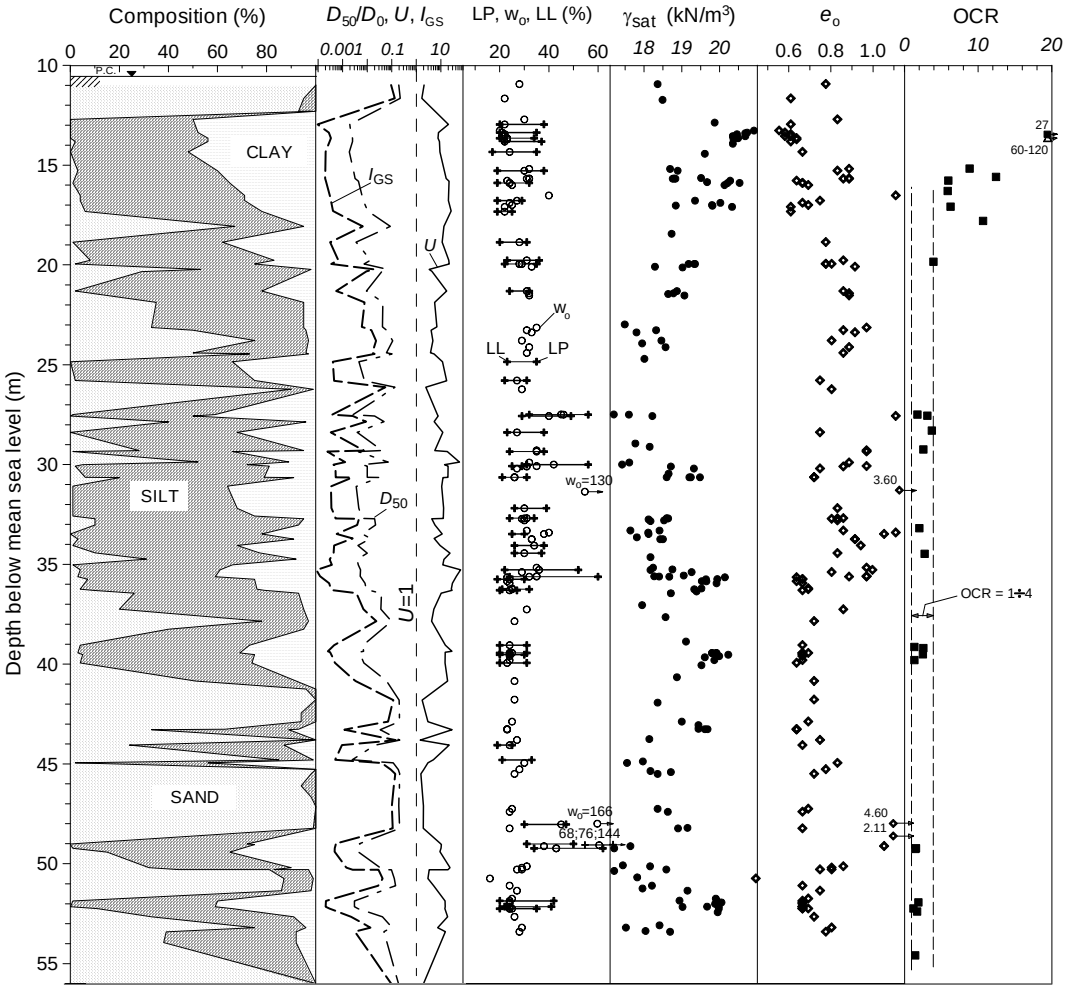

Figure 10. Soil profile, basic properties and stress history at the MTS.

3.2 *Stress history*

Overconsolidation ratio OCR, was evaluated on the basis of the estimated preconsolidation stress σ'_p from one-dimensional consolidation tests, carried out on CL specimens. Due to the very gradual transition to the virgin compression regime, the estimate of yielding stress was affected by high uncertainty and therefore not particularly reliable, excluding a few of more plastic silty-clay samples. No particular improvement in estimating σ'_p was unfortunately obtained by other methods (Grozic et al. 2003). A general decrease of OCR with depth can be observed in Figure 10, with the deeper formations remaining only slightly OC (OCR ≈ 1.2-3.7). The higher OCR values close to the top of the ground level are due to the *caranto*.

3.3 *Grain size index*

Since, at least up to the very silty clay fraction, all the sediments originated from one common basic material, namely siliceous-calcareous sands, it was attempted to establish some improved relationship between mechanical properties and the grading characteristics.

Venetian sands are relatively uniform but moving towards finer materials the soils become more graded and the grain-size curve displays a larger range, namely the coarser the materials, the lower non-uniformity coefficient U, whose range increases with decreasing D_{50}. On the basis of the above observations, it was sought to compare in Figure 11 all the pairs (D_{50}, U). Note that, even if both quantities show oscillations of approximately two orders of magnitude, the profiles of D_{50} and U are generally characterized by opposite trends with depth, namely, when D_{50} decreases the U increases and vice-versa. In order to take into account the coupled and opposite variation of D_{50} and U into a single parameter, a new grain-size index I_{GS} was proposed by Cola & Simonini (2002):

$$I_{GS} = \frac{D_{50} / D_0}{U} \tag{2}$$

where D_0 is a reference diameter equal to 1 mm.

In the laboratory characterization of the Venice soils, it was assumed that some significant time-independent material parameters could be related to I_{GS}, accounting for their grading properties. The significance of I_{GS} is limited here to the range $8 \cdot 10^{-5} \leq I_{GS} \leq 0.12$ and $CF < 25\%$.

3.4 *Mechanical characterization from laboratory tests*

An extensive laboratory investigation was carried out on the samples belonging to all the three groups. The experimental program consisted mainly of one-dimensional compression tests, drained and undrained triaxial tests (using in some tests a non-contact measurement system) and resonant column tests with a "fixed-free" apparatus. Shear wave velocity measurements have been performed on some samples using a bender element system in the triaxial apparatus. As already observed in section 2.3 the main difficulty in preparing the experimental program was the selection of relatively homogeneous samples representative of the three classes of soil.

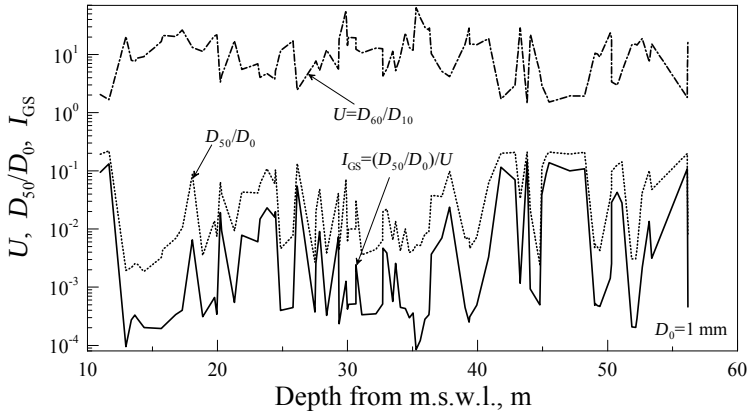

Figure 11. Grain size index versus depth at MTS.

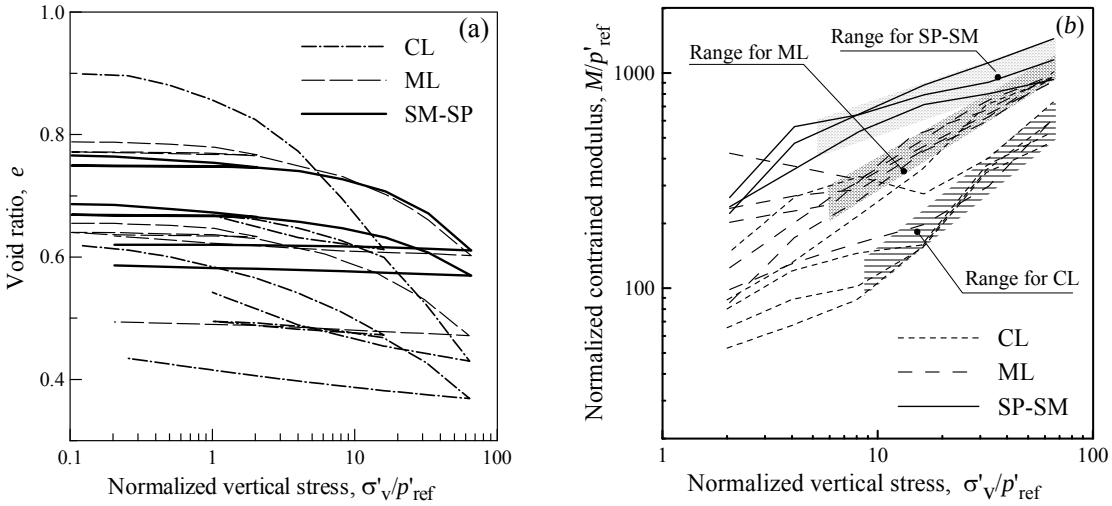

Figure 12. Void index (*a*) and normalized constrained modulus (*b*) vs normalized vertical stress for some 1-D compression tests on CL, ML and SP-SM soils.

3.4.1 *One dimensional compression*

Figure 12*a* report some typical 1-D compression curves of CL, ML and SP-SM samples. The response has been interpreted in terms of constrained modulus M as a function of vertical effective stress σ'_v (Janbu 1963),

$$\frac{M}{p'_{ref}} = C \cdot \left(\frac{\sigma'_v}{p'_{ref}} \right)^m \tag{3}$$

where C and m are two experimental constants and p'_{ref} a reference stress (p'_{ref} =100 kPa).

Figure 12*b* shows the trend of M as a function of σ'_v/p'_{ref} for the three classes of soil. The lowest values correspond to the CL class whereas the highest correspond to the SM-SP class.

The experimental constants C and m were related to the grain size index I_{GS} through the following equations:

$$C = (270 \pm 30) + 56 \cdot \log I_{GS} \tag{4}$$

$$m = (0.30 \pm 0.10) - 0.07 \cdot \log I_{GS} \tag{5}$$

Figures 13*a*,*b* show the trend of C and m as a function of I_{GS}.

An attempt to describe the one-dimensional compression of Venetian soils using a unified constitutive model was recently proposed by Biscontin et al. (2006).

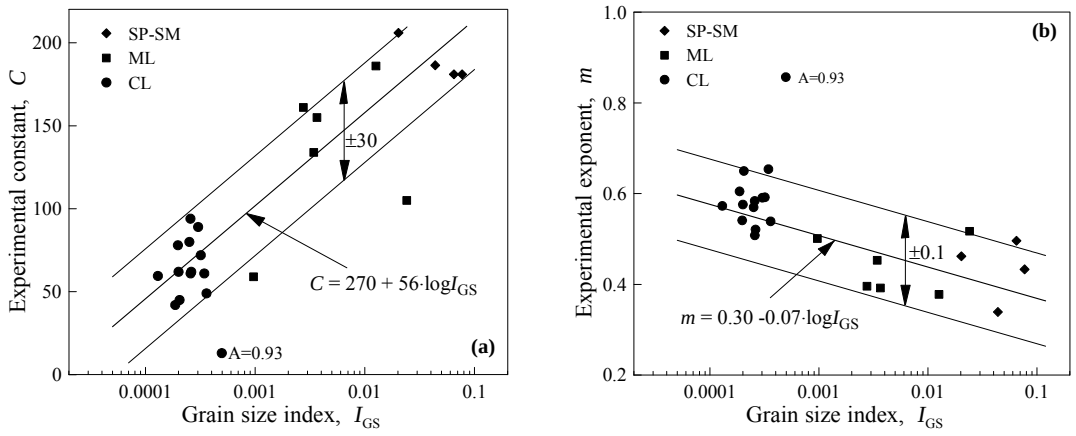

Figure 13. Material constants C (*a*) and m (*b*) as a function of grain-size index.

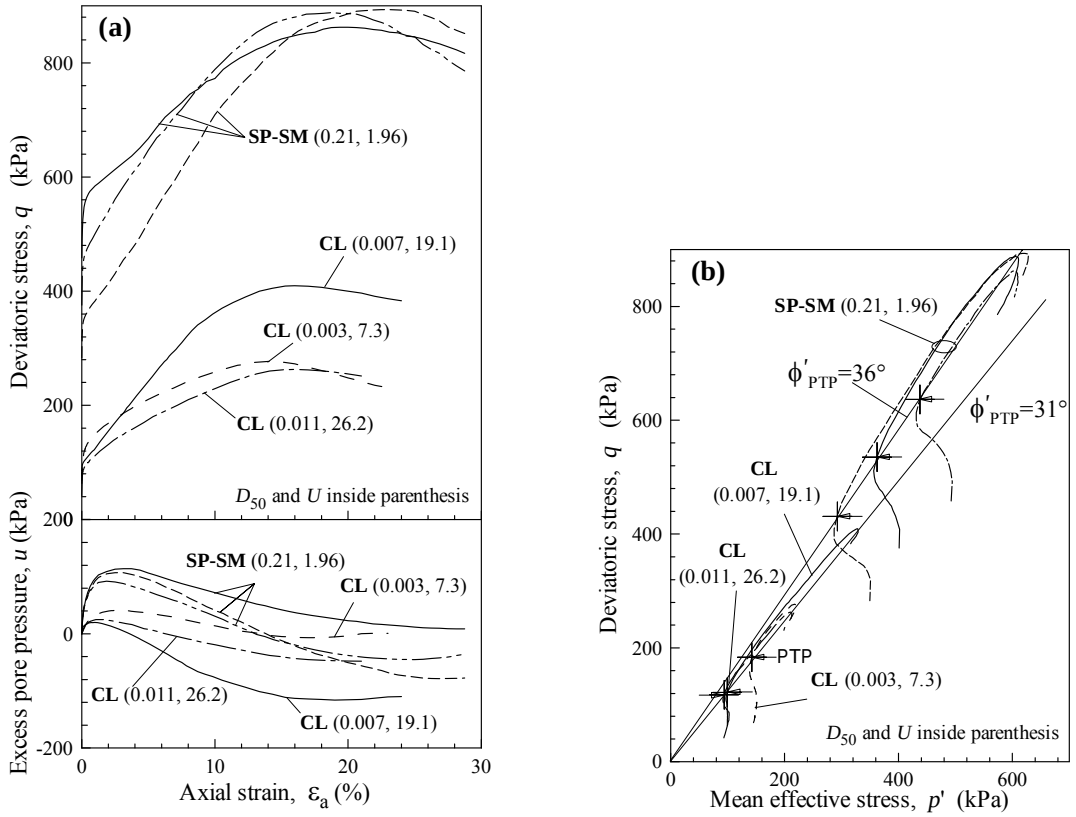

Figure 14. Typical undrained triaxial behaviour for SP-SM and CL soils: (*a*) q and u versus axial strain, (*b*) p'-q stress paths.

3.4.2 *Critical state*

Typical results of TX-CK_0U tests for the extreme classes SM-SP and CL are shown on Figure 14*a* in terms of deviatoric stress q *vs.* axial strain ε_a and pore pressure u *vs.* ε_a. Figure 14*b* sketches the corresponding stress-paths in the p'-q plane (p'=mean effective stress).

The evolution of u indicates the presence of both contractant and dilatant phases: the Phase Transformation Point (Tatsuoka & Ishihara 1974; Ishihara et al. 1975) marks the end of the contractant phase, after which the sample exhibited dilatant behavior.

Non-dilative response was observed only in a few of the tests performed on samples with higher clay content, but this behavior cannot be considered as representative of typically Venetian soils. The critical state angle ϕ'_c is reported in Figure 15 as a function of I_{GS}, distinguishing among the three soil classes and between drained (D) and undrained (U) tests. As expected, higher values are due to sands (34°- 39°) whereas silty clays show lower values (30°-34°). Critical angle of silts covers a larger range, reaching also the upper values of sands. It is interesting to notice the good correspondence between ϕ'_{PTP} and ϕ'_c, with scatter from the average value not exceeding ±2°, without any particular distinction among the three classes of soil and type of test.

The parameters e_{ref} = void ratio at p'_{ref} and λ_c = slope of the critical state line in the plane e-logp' were also estimated and two regression lines, one for SM-SP-ML the other for CL, determined: the pair (e_{ref}, λ_c) turned out to be equal to 0.918 and 0.066 for SM-SP-ML and 0.818 and 0.107 for CL, respectively (Cola & Simonini 2002). The trends, evaluated in the range between $8 \cdot 10^{-5} \le I_{GS} \le 0.12$, are characterized by the following expressions:

$$\phi'_c = (38.0 \pm 2.0) + 1.55 \cdot \log I_{GS} \qquad (°) \tag{6a}$$

$$\lambda_c = (0.152 \pm 0.04) - 0.037 \cdot \log I_{GS} \tag{6b}$$

$$e_{ref} = (1.13 \pm 0.10) + 0.10 \cdot \log I_{GS} \tag{6c}$$

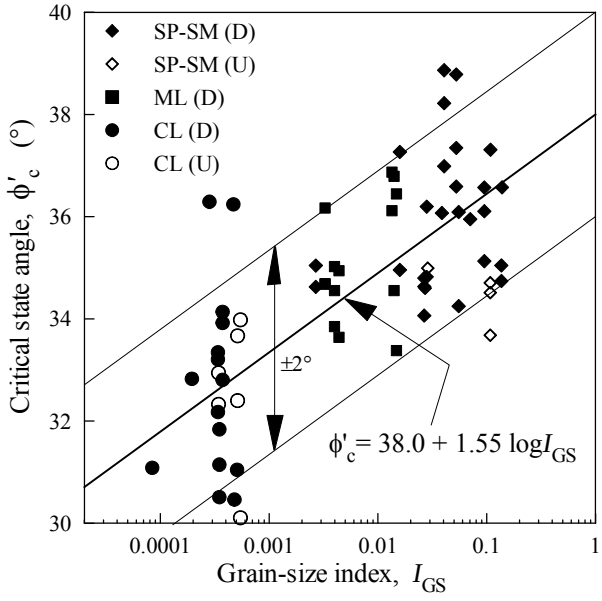

Figure 15. Critical state angle as a function of grain-size index.

It is interesting to point out that, before using the above correlations between critical state parameters and I_{GS}, attempts have been made to relate the same parameters singularly to D_{50} and U. The results indicated that ϕ'_c, λ_c, e_{ref} are a function of both quantities but with opposite effects: for example, ϕ'_c increases with D_{50} and decreases with U.

3.4.3 *Peak strength and state parameter*

Figure 16 shows the maximum dilation rate $\left(-d\varepsilon_v/d\varepsilon_a\right)_{max}$ measured in drained triaxial compression against the mean effective stress at failure p'_f. The same figure displays also the data of a few samples showing contractant response: in these cases the dilatancy values were set to zero and the points were drawn on the p'_f axis.

Features to note are:

- A general decrease of $\left(-d\varepsilon_v/d\varepsilon_a\right)_{max}$ with p'_f is observed for both sandy and silty soils. The shaded area includes the majority of data from tests on sands and silts, while the few data outside this area are due to silts with high clay fraction (CF is labelled above the dots);
- No particular distinction is evident between the sand and silt behaviour;
- Dilatancy vanishes at stress levels beyond about 1 MPa in all samples;
- The very silty clays are characterized by very low dilatancy with no particular trend related to p'_f.

Using the Bolton's expressions (1986 1987):

$$\left(-\frac{d\varepsilon_v}{d\varepsilon_a}\right)_{max} = 0.3 I_R \qquad (7a)$$

where the parameter I_R is:

$$I_R = D_R \cdot \left[\left(Q - \ln p'_f\right) - 1\right] \qquad (7b)$$

with $D_R=(e_{max}-e)/(e_{max}-e_{min})$ the relative density and Q an experimental constant (Bolton suggested Q = 10 for quartz and feldspar sands and 8 for limestone), the limits of the shaded area are marked using the values of $I_R = 0.7 \cdot \left[\left(9 - \ln p'_f\right) - 1\right]$ and $I_R = 0.5 \cdot \left[\left(9 - \ln p'_f\right) - 1\right]$. This implies that the measured dilatancy should correspond to a relative density D_R in the range 0.5-0.7 with the parameter Q equal to 9.

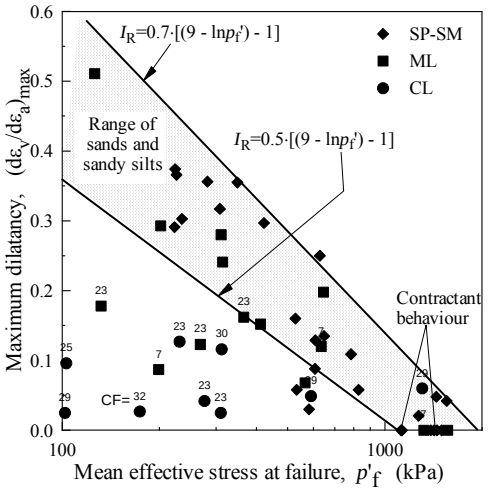

Figure 16. Maximum dilatancy versus mean effective stress at failure in triaxial tests.

According to Bolton the peak angle ϕ'_P is similarly related to parameter I_R by:

$$\phi'_P - \phi'_c = 3I_R \tag{8a}$$

that may be adapted to the Venice soils as follows:

$$\phi'_P - \phi'_c = 3.9\left[(9 - \ln p'_f) - 1\right] \tag{8b}$$

The value 3.9, used here instead of 3 suggested by Bolton, may be partially justified by considering that the Venetian sands and silts are composed of angular grains, thus providing a higher degree of interlocking, whereas the data reported by Bolton are mostly referred to sands characterized by a lower degree of angularity (e.g. Lee & Seed 1967).

The state parameter ψ (Wroth & Bassett 1965; Been & Jefferies 1985; Been et al. 1991) defined here as:

$$\psi = e - e_{ref} + \lambda_c \log \frac{p'}{p'_{ref}} \tag{9}$$

was also calculated on the basis of the void ratio e_{ref} corresponding to the reference pressure p'_{ref} =100 kPa on the experimental critical state line. According to Wood et al. (1994) the state parameter can be related by the expression:

$$\phi'_P = \phi'_c - \beta \cdot \psi \tag{10}$$

where experimental value of β for sands and silts results equal to 40, as shown in Figure 17.

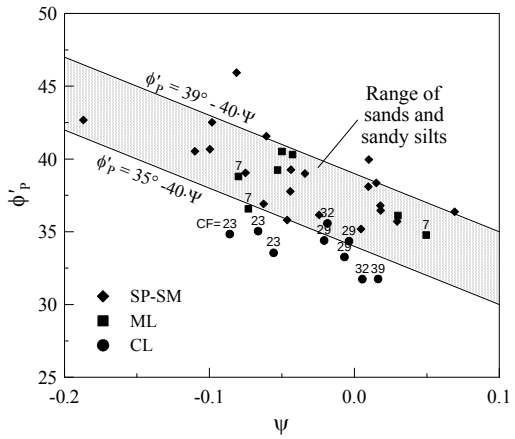

Figure 17. Peak angle in triaxial compression as a function of the state parameter.

3.4.4 *Very small strain behavior*

The maximum stiffness G_{max} was determined on specimens from the three classes of soils, using resonant column tests (RC) and shear wave velocity measurements performed in triaxial tests using bender elements (BE). The experimental data were interpreted as function of p', OCR and e (Hardin & Black 1969, Hardin & Drnevich 1972). For sands, low-plasticity and slightly OC cohesive soils, the effect of OCR is considered negligible (Hardin & Drnevich 1972) and G_{max} can be related to e and p' by the expression:

$$\frac{G_{max}}{p'_{ref}} = D \cdot \frac{(2.97 - e)^2}{(1+e)} \cdot \left(\frac{p'}{p'_{ref}} \right)^n \tag{11}$$

where D is a material constant and n is an exponent.

Figure 18 depicts the ratio $G_{max}/(f(e) \cdot p'_{ref})$ as a function of normalized mean stress p'/p'_{ref}, distinguishing among the soil types and the test types. An exponent n equal to 0.60 could be reasonably assumed as representative of the trend for all data.

As shown in Figure 19, the dependence of the material constant D on I_{GS} was assessed and fitted by the equation:

$$D = (470 \pm 50) + 26.3 \cdot \log I_{GS} \tag{12}$$

Note that I_{GS} is once more capable of expressing the dependence of G_{max} on the three classes of soils.

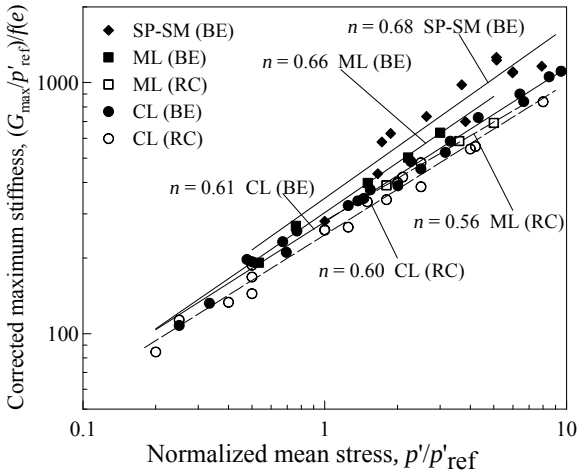

Figure 18. Corrected maximum stiffness as function of mean effective stress.

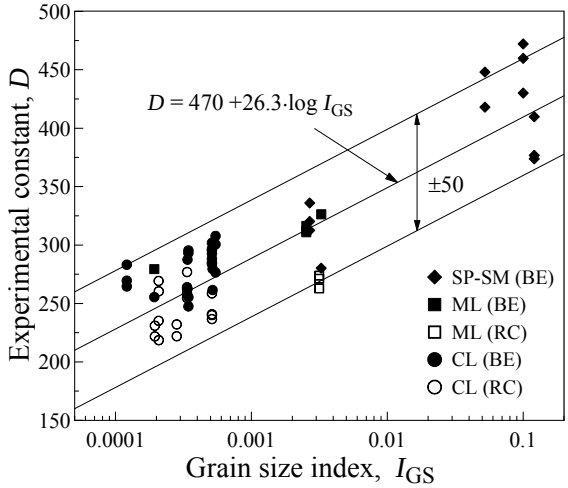

Figure 19. Material constant D as a function of grain-size index.

3.4.5 *Stiffness at small-intermediate strains*

Trends of secant shear stiffness determined in undrained compression (C) and extension (E) tests for some CL samples are displayed *vs*. shear strain ε_s in Figure 20*a* (Cola & Simonini 1999). The tests were performed in a special triaxial cell equipped with internal non-contact displacement sensors. The undisturbed CL specimens were reconsolidated at the in-situ K_0 stress state before increasing the deviatoric stress up to failure.

A general decrease of shear stiffness is observed, with lower values for compressions above $\varepsilon_s \approx 0.02\%$. The limit of linear elastic behavior seems to be in the range of strains between $\approx 0.003\%$ and $\approx 0.006\%$, for compression and extension respectively. Considering the plasticity index, the overconsolidation of the Venetian silts and strain rate applied in the laboratory tests, the above limits of linear behavior appear to be in agreement with those obtained by other researchers (e.g. Dobry & Vucetic 1987, Tatsuoka & Shibuya 1992; Leroueil & Hight 2002).

Small unload-reload cycles were applied in some tests during the shearing stage in order to check the effects of straining on reversible behavior. The results are plotted in Figure 20*b* (specimens VE5-C and VE5-E) in terms of secant shear stiffness G_{load} and initial stiffness in the reloading phase G_{reload} against shear strain ε_s. Within limits of up to $\varepsilon_s=1\%$, to which corresponds relatively high stress levels $\eta/\eta_{max}=0.92$ and $\eta/\eta_{max}=0.68$ in compression and extension respectively, the reloading modulus shows a slight decreasing trend. Little damage of soil structure should therefore develop up to a shear strain of 1%.

3.4.6 *Anisotropy in elastic range*

The stress-strain relation of a cross-anisotropic elastic material given by Graham & Houlsby (1983) is:

$$\begin{bmatrix} \delta p' \\ \delta q \end{bmatrix} = \begin{bmatrix} K^* & J \\ J & 3G^* \end{bmatrix} \begin{bmatrix} \delta \varepsilon_v \\ \delta \varepsilon_s \end{bmatrix} \tag{13}$$

where J is a coupling modulus and asterisks have been added to K and G to show that the material is no longer isotropic.

Considering that the volumetric strain increment $\delta\varepsilon_v$ is zero in undrained compression tests, it is possible to write:

$$\frac{\delta u}{\delta q} = \frac{1}{3} - \frac{J}{3G^*} \tag{14}$$

If J=0, i.e. isotropic elastic soil, the ratio between pore pressure and deviatoric stress increments must be equal to 1/3. For materials stiffer horizontally than vertically, the value of J

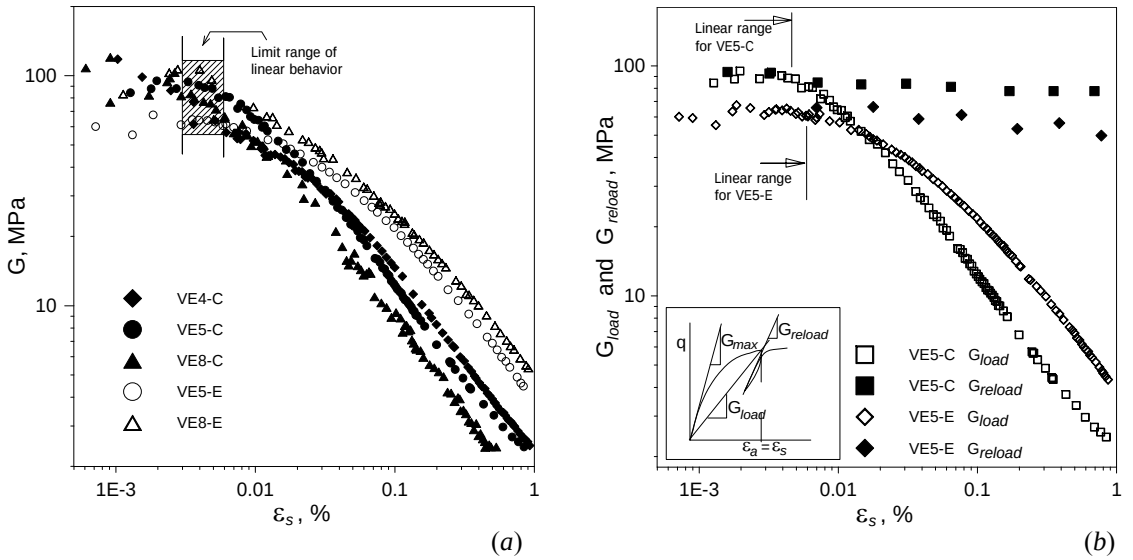

Figure 20. (*a*) Shear modulus vs. shear strain and (*b*) comparison between secant and reloading modulus in undrained compression and extension triaxial tests.

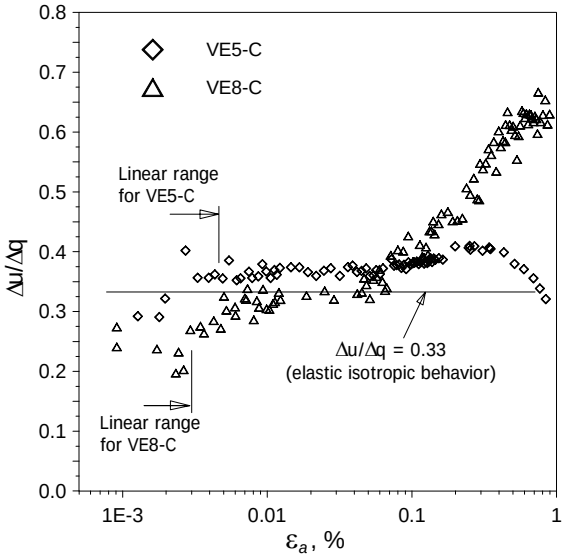

Figure 21. $\Delta u/\Delta q$ ratio vs. ε_a in undrained compression.

is negative and the pore pressure ratio $\Delta u/\Delta q$ should therefore exceed 1/3.

Figure 21 reports $\Delta u/\Delta q$ as a function of axial strain for samples VE5-C and VE8-C, already mentioned in section 3.4.5, together with the estimated limits of pre-yield behaviour (Cola & Simonini 1999). Within these limits the soil seems to be characterized by a small anisotropic behavior with stiffer response in a vertical direction.

3.4.7 *Consolidation and secondary compression*

Primary consolidation coefficient of CL-ML samples is rather high and in the range 10^{-7}–10^{-5} m^2/sec, thus confirming that Venetian silts are relatively free draining materials.

Secondary compression coefficient $C_{\alpha e}=\Delta e/\Delta \log t$ estimated from the oedometric tests is reported as function of vertical stress in Figure 22*a*. Although the tests are carried out on all types of soils, $C_{\alpha e}$ does not exhibit great variation being the index more affected by the stress history rather than from the grain-size composition.

According to Mesri & Godlewski (1977) and Mesri et al. (1995), the ratio $C_{\alpha e}/C_c$ (C_c is the local slope of the e-logσ'_v curve) is not dependent on the stress level or material density. Mesri et al. suggested a small dependence from soil composition, $C_{\alpha e}/C_c$ varying from 0.02 to 0.05 moving from granular soils to silts and to organic clays, but for the Venetian soils this ratio does not appear particularly dependent on grain-size composition: from Figure 22*b* it appears that above ratio of the three classes CL, ML and SP-SM fall approximately in the same range. The best fitting provides $C_{\alpha e}/C_c$ =0.028 with negligible differences between the classes CL, ML and SP-SM. A higher value equal to 0.031 is obtained for the few CH-OH soils.

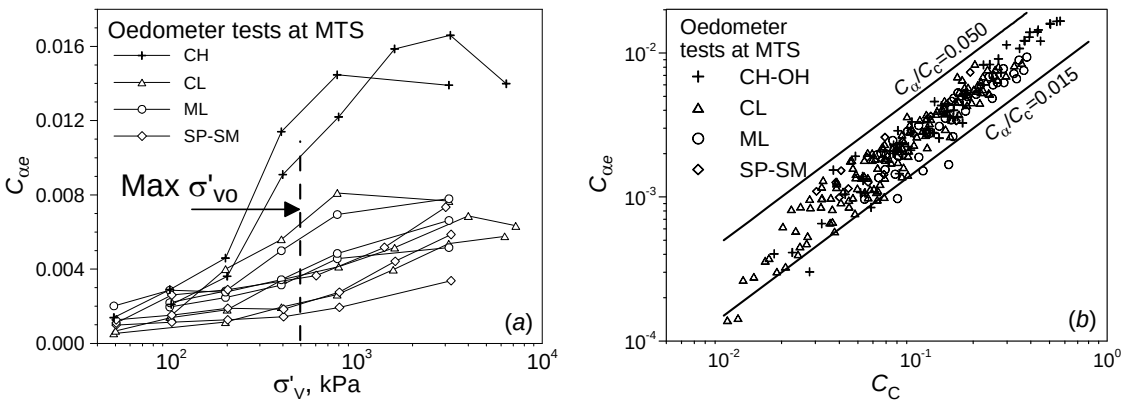

Figure 22. (*a*) Secondary compression index vs. vertical stress and (*b*) vs. compression index from oedometer tests.

3.5 *Characterization from site testing: piezocone and dilatometer applicability*

One of the aims of the MTS was to evaluate the applicability of CPTU and DMT for extensive soil characterization at the three inlets (and, eventually to provide a site-specific calibration), thus avoiding the use of more expensive borehole and laboratory testing as well as the scale effects inherent in these highly heterogeneous soils.

The CPTUs at the MTS were carried out using the standard Dutch cone provided by the pore pressure transducer located along the shaft just behind the cone (Torstensson 1975, 1977) with a ratio *a* between net and total area equal to 0.83.

The following symbols have been used in the interpretation of the CPTU:

q_c = cone resistance;
u_2 = pore pressure measured at the cylindrical extension of the cone;
f_s = measured sleeve friction;
$q_t = q_c + (1\text{-}a)\, u_2$ = corrected cone resistance;
$q_n = q_t - \sigma_{vo}$ = net corrected cone resistance (σ_{vo} = total overburden stress);
$\Delta u_2 = u_2 - u_o$ = excess pore pressure, where u_o is water pore pressure in a hydrostatic condition;
$R_f = 100\, f_s/(q_t - \sigma_{vo})$ = normalized sleeve friction ratio;
$B_q = \Delta u_2 /(q_t - \sigma_{vo})$ = pore pressure ratio.

The standard DMT test procedure (Marchetti 1975, 1980) was utilized at the MTS, recording the gas pressure p_0 to lift the membrane off the sensing device located just beneath the membrane and the gas pressure p_1 to cause 1 mm deflection. From these two pressure readings Marchetti derived the three index parameters, namely the material index $I_D = (p_1 - p_0)/(p_0 - u_0)$, the horizontal-stress index $K_D = (p_0 - u_0)/\sigma'_{vo}$ and the dilatometric modulus $E_D = 34.7(p_1 - p_0)$ where σ'_{vo} is the in-situ vertical effective stress, and subsequently a series of empirically derived properties through correlations based on the above three index parameters (e.g. Totani et al. 1999).

The results of two typical tests SCPTU19 and MDMT2, carried out at closer distance, are shown in Figure 23 in terms of the profiles of q_t, f_s, u_2, p_0, p_1 and V_s, where the latter is the shear wave velocity measured at various depths by the SCPTU and by the CHT.

Sharp variations of q_t, f_s and u_2 are observed; more particularly u_2 remains below the hydrostatic level not just in the *caranto* but also in some cases in the sandy layers. This effect has been observed in the special circumstances of dense cohesionless soil that exhibits dilation when sheared (Wroth 1984). B_q rarely exceeds 0.4 at MTS, whereas in other sites higher values have been observed.

The p_0 and p_1 profiles are characterized by the continuous and coupled oscillations of the two pressures, thus confirming the high degree of heterogeneity already shown by SCPTU19.

In CHT an increasing trend of V_s with depth, from 150 m/s up to 300 m/s at 50 m below m.s.l., is noted with very small variations among the different soil formations. Some flapping of V_s, measured with SCPTU at depths from 29 to 34 m and 45 to 52 m, may be due to the presence of some thin peaty layers, which could influence the propagation of V_s across horizontal soil layering.

On the basis of laboratory test results, an evaluation of the applicability of CPTU and DMT to estimate some relevant geotechnical properties is considered and discussed in the following sections. Other information can be found in Ricceri et al. (2002).

3.5.1 *Soil classification*

Soil classification with CPTU can be obtained by using q_t and f_s alone (Olsen & Farr 1986; Robertson 1990) or with u_2 (Senneset et al. 1982; Robertson 1990).

All the classification methods are based on empirical charts, with the most widely accepted being Robertson's where the soils are grouped into 9 classes, accounting also for OCR. Figure 24 reports the CPTU data superimposed onto Robertson's chart (in terms of q_t vs. R_f and in terms of q_t vs. B_q), dividing the soils into the four classes, SM-SP, ML and CL and organic soils. The proposed subdivision seems relatively suitable for the classification of the Venetian soils, which mostly belong to the groups 4, 5 and 6.

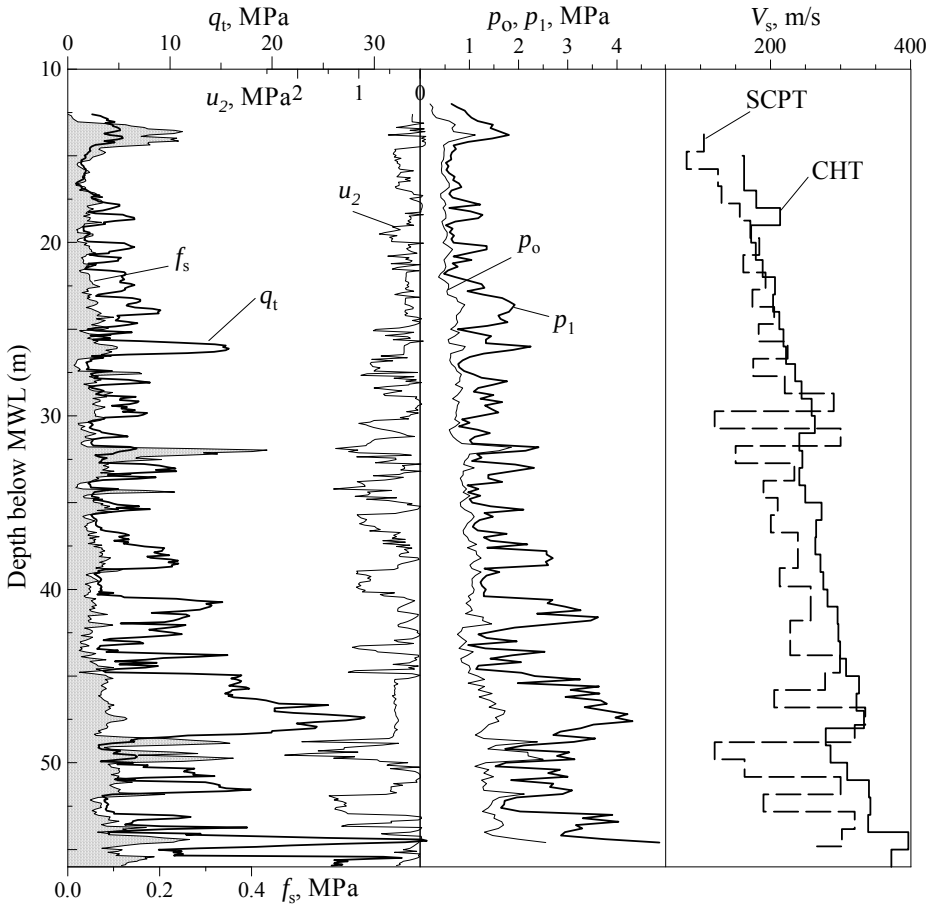

Figure 23. Profiles of q_t, f_s, u_2, p_o, p_1 and V_s at MTS.

The material index I_D was originally used as approximate parameter for identifying the soil type, i.e. $I_D \leq 0.6$ for clay, $0.6 < I_D < 1.8$ for silt and $I_D \geq 1.8$ for sand. However, it was later recommended to combine the material index I_D with E_D for better soil classification.

Figure 25 summarizes the data obtained from the MTS and plotted on the improved chart

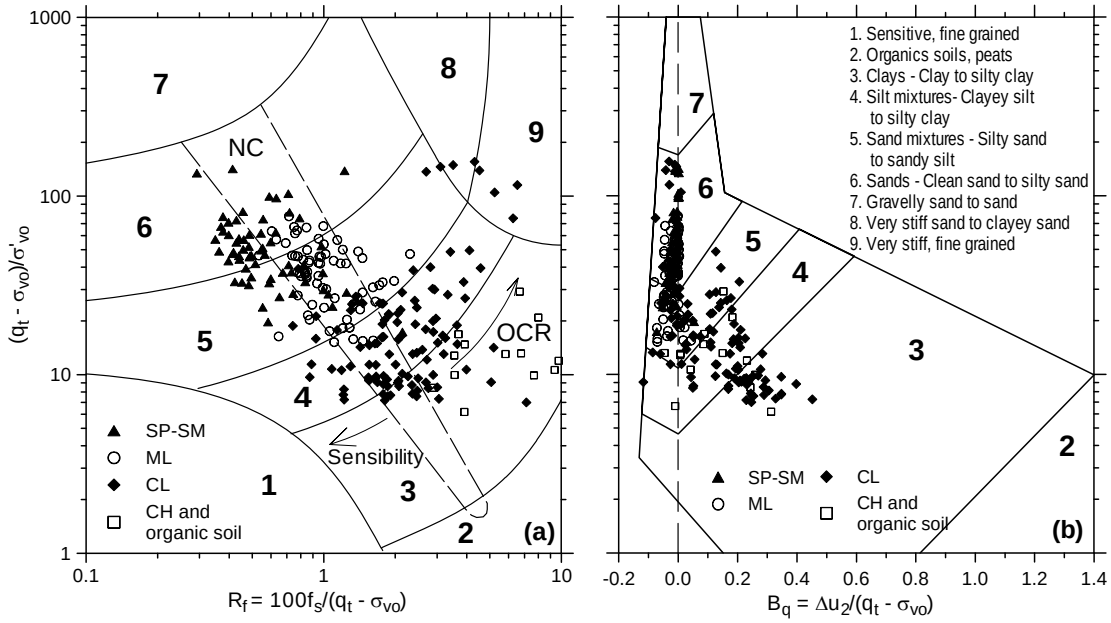

Figure 24. Classification with the Robertson's charts.

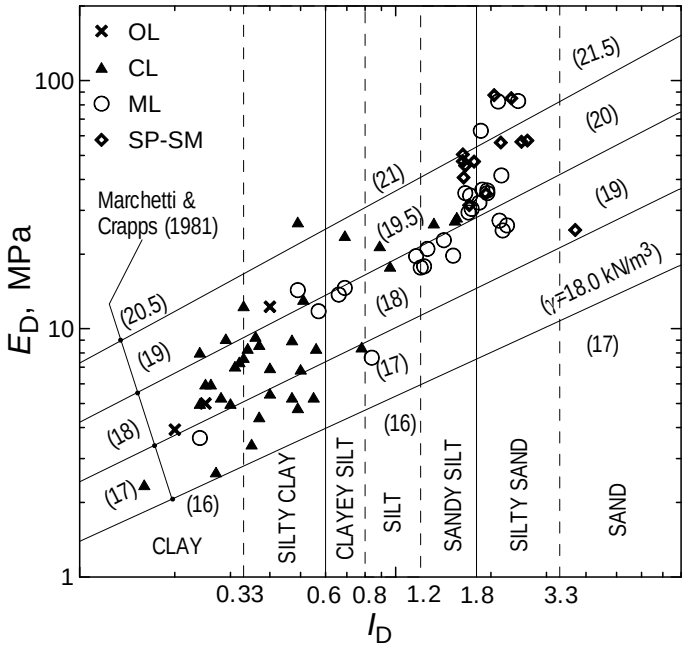

Figure 25. Classification by means of Marchetti and Crapps chart.

proposed by Marchetti & Crapps (1981). The two extreme classes of soil, namely the silty clay (CL) and silty sand (SM-SP) appear to be better defined than those of silts (ML).

Marchetti & Crapps soil classification chart provides indications about the unit weight of soil. Comparing the γ predicted with that measured in the laboratory, the range of maximum scatter around the average values does not exceed 15%. Nevertheless, the chart tends to overestimate γ in CL soils while underestimating that of SM-SP class.

3.5.2 *Overconsolidation ratio*

The level of u_2 generated during cone penetration, and consequently the value of B_q, are functions of the type of soil and of OCR.

In order to verify if a possible relationship between OCR and B_q exists, the OCR's values determined from 1-D compression tests on CL samples were plotted versus B_q in Figure 26. A general decrease of OCR along with an increase of B_q can be observed, but no reliable correlation between these two quantities can be established, the level of u_2 being much more dependent on soil type than on OCR.

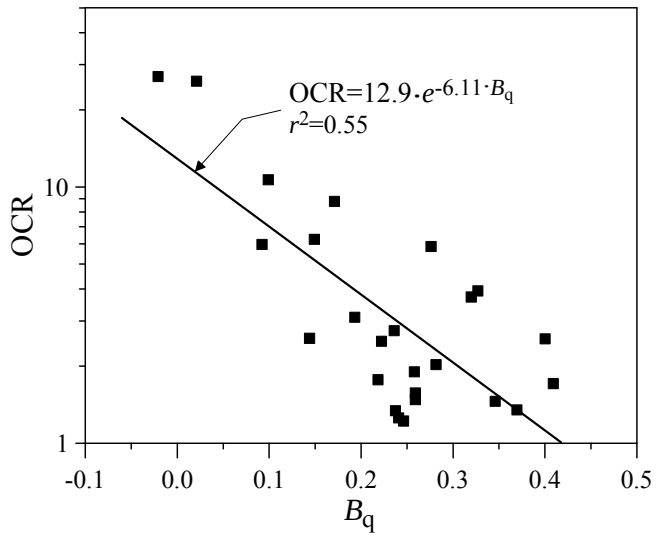

Figure 26. Relationship between overconsolidation and pore pressure ratios.

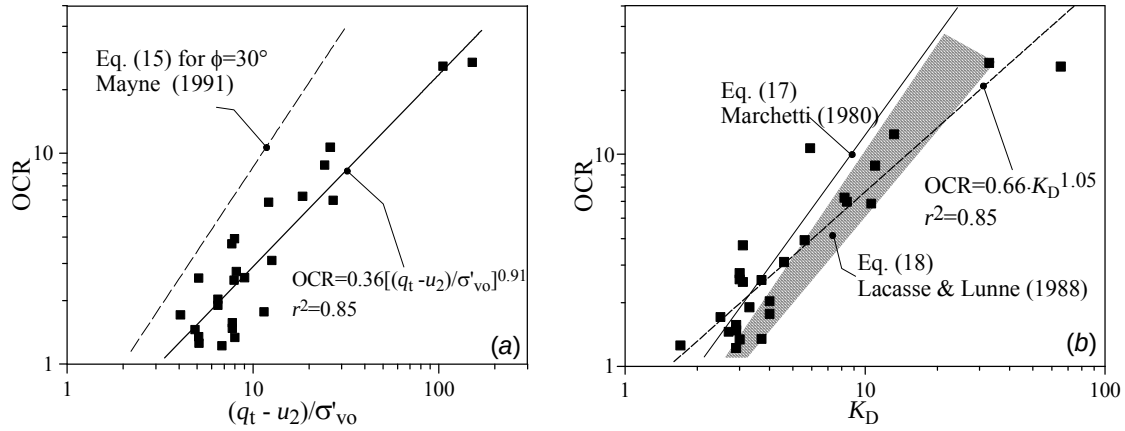

Figure 27. Overconsolidation ratio versus $(q_t\text{-}u_2)/\sigma'_{vo}$ (*a*) and versus horizontal stress index (*b*).

Another attempt to link OCR with CPTU results could be performed as suggested by Mayne (1991), who proposed a relationship between OCR and the ratio $(q_t\text{-}u_2)/\sigma'_{vo}$ on the basis of the coupled use of cavity expansion theory and of the MCC model:

$$\mathrm{OCR} = 2\left\{\left(\frac{q_t - u_2}{\sigma'_{vo}}\right)\Big/\left[1.95\left(\frac{3\sin\phi'_c}{6-\sin\phi'_c}\right)+1\right]\right\}^{1.33} \tag{15}$$

where $3\sin\phi'_c/(6-\sin\phi'_c)$ is the slope of critical state line in the (p',q) plane.

The data reported in Figure 27*a* confirm the relation between OCR and the ratio $(q_t\text{-}u_2)/\sigma'_{vo}$. The curve given by Mayne's theoretical approach for a friction angle of 30°, characteristic of the Venetian clayey silts, represents approximately an upper limit of OCRs.

Figure 27*a* also reports the best regression fit obtained on experimental data, with the expression:

$$\mathrm{OCR} = 0.36\left(\frac{q_t - u_2}{\sigma'_{vo}}\right)^{0.91} \tag{16}$$

which could be used to predict tentative profiles of OCR in the slightly over consolidated range.

The estimation of OCR for clays was proposed by Marchetti relating K_D to OCR from oedometer tests with the following correlation:

$$\mathrm{OCR} = \left(0.5K_D\right)^{1.56} \tag{17}$$

The use of correlation (17) is restricted to materials with I_D<1.2, free of cementation which have experienced simple one-dimensional stress histories.

Among the improved relationships available in literature, that proposed by Lacasse & Lunne (1988):

$$\mathrm{OCR} = 0.225K_D^{\,1.35\text{–}1.67} \tag{18}$$

takes into account a large range of soil plasticity in the exponent, that varies from 1.35 for plastic clays up to 1.67 for low plasticity materials.

The applicability of correlations (17) and (18) to MTS data was verified in Figure 27*b*. The Marchetti correlation seems to provide a rather good estimation of OCR at the lowest values of K_D. Large differences compared to laboratory results occur at higher horizontal stress indexes (K_D>10), that is, for the highly OC *caranto* at shallow depths. No improvement of data relating to any of the K_D range was obtained by adopting the Lacasse & Lunne relationship.

If we apply the power regression to all our data independently of I_D and stress history we have the following relationship:

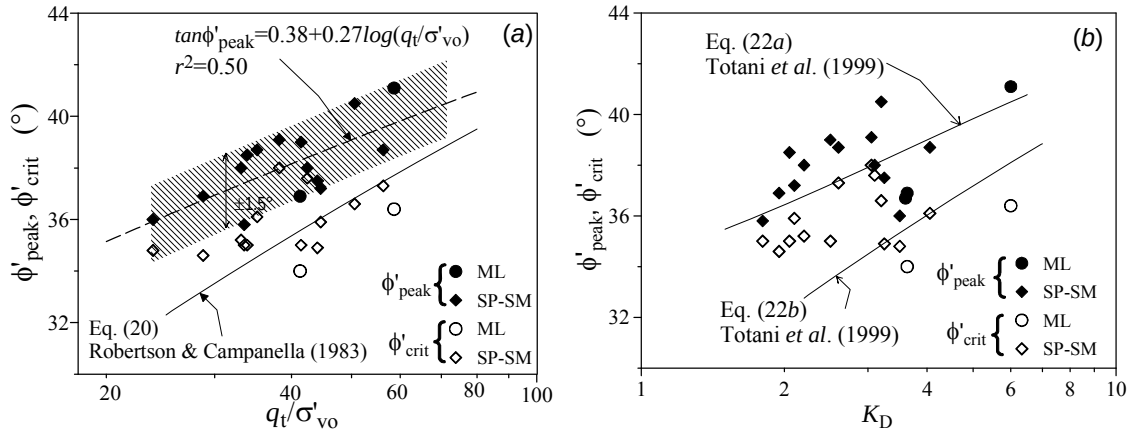

Figure 28. Friction angles vs. the normalized cone resistance (*a*) and vs. the horizontal-stress index (*b*) in sands and silty sands.

$$\mathrm{OCR} = 0.66\, K_D^{\,1.05} \tag{19}$$

which could provide, as similar to the piezocone, an OCR prediction in the range $1.7 < K_D < 70$.

3.5.3 *Friction angle*

The relationship due to Durgunoglu & Mitchell (1975) and modified by Robertson & Campanella (1983) is based on the correlation between ϕ', q_t and σ'_{vo}:

$$\phi' = \arctan\left[0.10 + 0.38 \log\left(\frac{q_t}{\sigma'_{vo}}\right)\right] \qquad (°) \tag{20}$$

A similar relationship was used in our case and the regression fitting:

$$\phi'_p = \arctan\left[0.38 + 0.27 \log\left(\frac{q_t}{\sigma'_{vo}}\right)\right] \pm 1.5 \quad (°) \tag{21}$$

is proposed in Figure 28*a*, where the shaded area defines the range of possible excursion between the upper and lower values of the peak angle ϕ'_p.

Observing a linear correlation between K_D and q_t, Marchetti adapted the relationship (20), thus presenting a new chart that provides ϕ'_p of sand from K_D. Recently Marchetti (from Totani et al. 1999) suggested two direct empirical correlations, which could be used to give lower and upper bounds of the range of possible friction angles:

$$\phi'_{max} = 31 + K_D/(0.236 + 0.066 K_D) \tag{22a}$$

$$\phi'_{min} = 28 + 14.6 \cdot \log K_D - 2.1 \cdot (\log K_D)^2 \tag{22b}$$

A comparison between laboratory values of peak and critical friction angles from triaxial tests on SP-SM and ML soils and the value predicted by Equations (22*a*, *b*) is plotted in Figure 28*b*: the fitting is rather limited showing a poor dependence of friction angle on K_D.

3.5.4 *Undrained strength*

From q_t the undrained shear strength c_u can be determined by applying the bearing capacity equation to the cone resistance. Hence, we have:

$$c_u = \frac{q_c - \sigma_{vo}}{N_k} \tag{23}$$

where N_k is the cone bearing capacity factor. Several theoretical approaches are available for N_k

(Yu & Mitchell 1998), the latter being theoretically characterized by a large range of variation, between 11 and 19 for NC clays, approaching 25 for OC ones.

In the Venetian silty clays the process of penetration is partially drained and therefore the interpretation of cone resistance in terms of undrained strength is rather questionable (e.g. Randolph 2004). Nevertheless, on the basis of c_u measured in the laboratory, tentative values of N_k were calculated for CL formations. The result is shown in Figure 29*a*. The scatter around the average value of 8.5 is relatively large; equation (23) can be therefore used only for a possible rough estimate of c_u.

Considering the dependence of c_u/σ'_{vo} on OCR, Marchetti proposed a correlation between c_u and K_D:

$$\frac{c_u}{\sigma'_{vo}} = 0.22\left(0.5K_D\right)^{1.25}. \tag{24}$$

Correlation (24) was recommended only for material with I_D<1.2 and simple loading history.

Undrained strength from triaxial tests is plotted against K_D in Figure 29*b*: a general increase of c_u as a function of K_D is appreciated. It may therefore be suggested that the original correlation could be utilized for a preliminary estimate of c_u for all the range of K_D.

3.5.5 *Maximum shear stiffness*

Correlations were proposed between CPT resistance and G_{max} for a large variety of soils (Baldi et al. 1989; Mayne & Rix 1993; Hegazy & Mayne 1995). The major criticism to all these correlations is that G_{max} is a parameter determined at very small shear strain levels whereas q_t is a quantity measured at large deformations involving yielding and failure of the soil surrounding the cone. However, as pointed out by Mayne & Rix (1993), for a given soil, both quantities show similar dependence on the same parameters, namely the mean effective stress level and void ratio.

The reconstruction of the *e* profile is a difficult task. The advantage of using the CPTU is given by the continuous profile of B_q which, in these soils, is mainly a function of pore size distribution rather than OCR. Therefore, the B_q profile may act as a simple substitute of *e* profile, in order to take into account soil type and its structural condition.

To analyze the dependence of G_{max} on q_t and B_q the data from the SCPT, CHT and from laboratory measurements performed with BE and RC (see section 3.4.4) were used (Simonini & Cola 2000). The data on Figure 30 show that an association between G_{max}, q_t and B_q is reasonably possible for Venetian soils. The following multiple regression function applied on data from all types of soils was selected:

$$G_{max} = 21.5q_t^{0.79}\left(1+B_q\right)^{4.59} \quad \text{(MPa)} \tag{25}$$

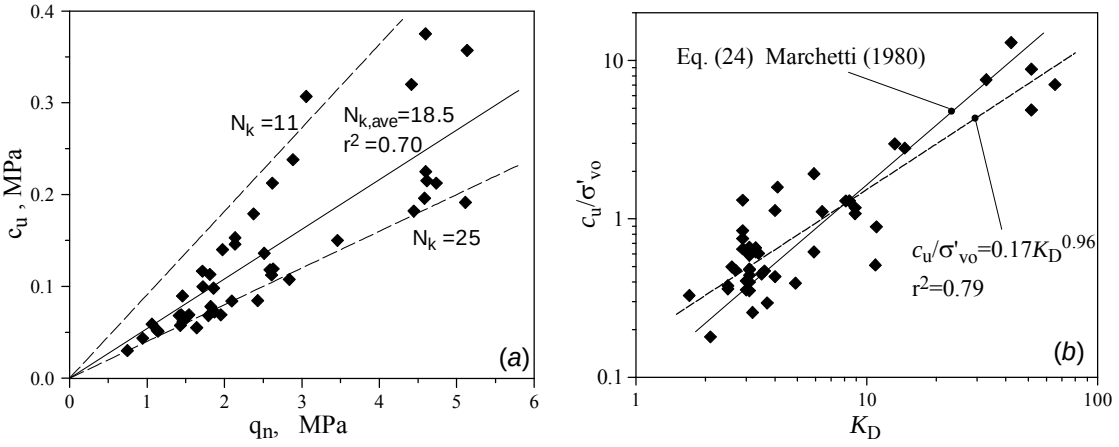

Figure 29. Undrained shear strength from triaxial tests vs. net cone resistance (*a*) and shear strength ratio versus horizontal stress index (*b*).

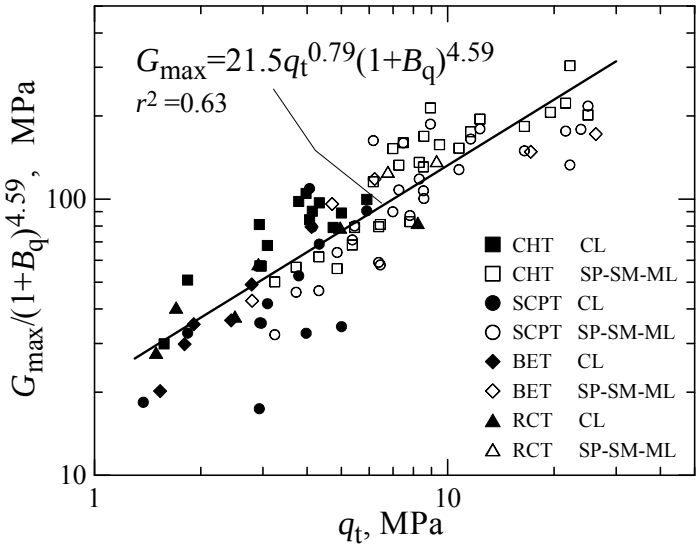

Figure 30. Relationship between maximum stiffness and CPTU parameters.

The very small-strain modulus can also be estimated from E_D. The ratio:

$$R_G = G_{max} / E_D \tag{26}$$

is, in some cases, expressed as a function of K_D or relative density (Jamiolkowski et al. 1988), but these relationships cannot be applied to all soils. Hryciw (1990) expressed G_{max} as a more general function of K_0, γ_{DMT} and σ'_{vo}, in which K_0 is given by the original Marchetti (1980) relationship:

$$K_o = \left(K_D / 1.5\right)^{0.47} - 0.6 \tag{27}$$

and γ_{DMT} is the total unit weight determined from DMT data by means of Marchetti & Crapps' chart.

As presented above the errors in estimating γ_{DMT} and K_0 for Venetian soil are not negligible. Consequently, we preferred to propose a direct relationship between R_G and I_D: the best fitting was found in the form of the logarithmic relationship between R_G and I_D, as shown in Figure 31. Using G_{max} data measured both in-situ and in the laboratory, the relationship can be written as:

$$R_G = 6.71 - 14.2 \log I_D \tag{28}$$

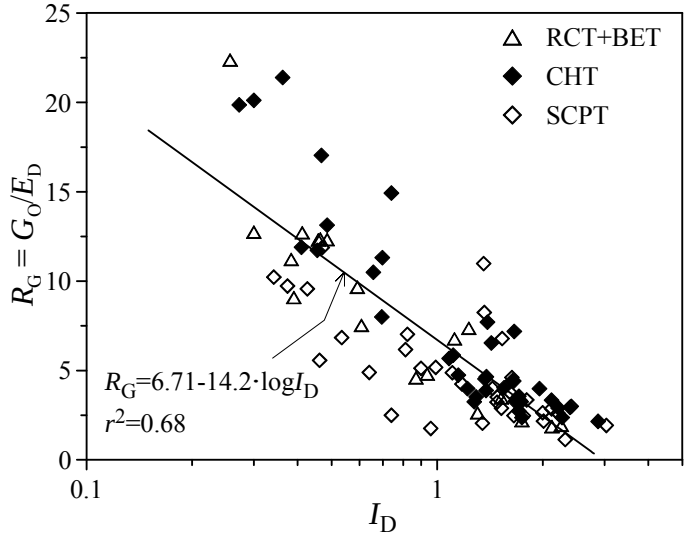

Figure 31. Relationship between R_G and material index.

4 THE TREPORTI TEST SITE

In order to measure in-situ the stress-strain-time properties and verify the above discussed applicability of SCPTU and DMT to characterize the Venetian soils, a comprehensive research program was recently launched.
It was concerned with the construction of a full-scale earth-reinforced cylindrical embankment over a typical soil profile in the Venice lagoon and with the measurement of relevant displacements of ground together with pore pressure evolution.

The project has been developed in the following steps:

a) selection of the typical test site in the lagoon area;
b) execution of site investigations;
c) installation of the monitoring system;
d) construction of the embankment;
e) monitoring the displacements and pore pressure during the embankment realization;
f) execution of laboratory investigations;
g) repetition of some in-situ tests after the completion of the embankment;
h) prosecution of monitoring for almost four additional years after embankment completion.
i) staged bank removal with monitoring of ground displacements in unloading condition.

The test site is located just outside Treporti, an old fishing village near the Cavallino shoreline, facing the North-Eastern lagoon (*TTS* in Figure 1).

4.1 *Site and laboratory investigations*

Figure 32 sketches the location of site investigations consisting of 10 CPTU with dissipation tests and 2 mechanical CPT (Gottardi & Tonni 2004); 10 DMT with dissipation tests (Marchetti et al. 2004); 6 seismic SCPTU/SDMT (Mayne & Mc Gillivray 2004); 4 boreholes. Undisturbed sampling was carried in the most cohesive formations out by using the classical Osterberg sampler. Two additional CPTU and four DMT have been also performed after completion of the embankment.

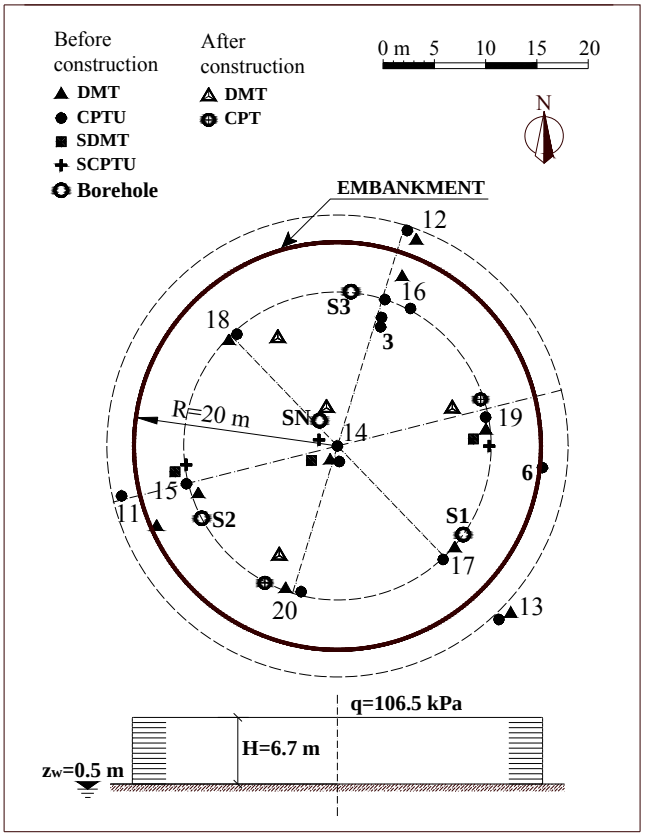

Figure 32. Embankment plan with location of site investigation tests.

On the Osterberg undisturbed samples standard laboratory tests have been carried out. Plastic liner samples were used for a detailed classification of soil profile.

4.2 *Monitoring instrumentation*

The instrumentation installed at TTS was designed to keep the following main quantities under control:

- surface vertical displacements using 7 settlement plates and 12 bench marks, the latter located outside the embankment area;
- surface vertical displacement by one GPS antenna, located in the centre of the embankment area and fixed to the central settlement plate;
- vertical deep displacements by means of 8 borehole rod extensometers;
- vertical strains, along with four verticals, using 4 special multiple micrometers;
- horizontal displacements by means of 3 inclinometers;
- pore water pressure in fine-grained soils by means of 5 Casagrande as well as 10 vibrating wire piezometers;
- total vertical stress beneath the loading embankment by means of 5 load cells.

Figures 33 and 34 show the instrumentation position and a schematic soil profile, which is described in the next sections.

To measure the vertical displacements throughout the foundation ground very precisely, multiple micrometers, capable of measuring vertical displacements at 1 m intervals with an adequate degree of accuracy of 0.03 mm/m (Kovari & Amstad 1982), were selected.

4.3 *Embankment construction*

Three-meter long prefabricated vertical drains were first installed to speed up the drainage of a shallow clay layer (about 1.5 thick) and to prevent possible lateral soil spreading during construction.

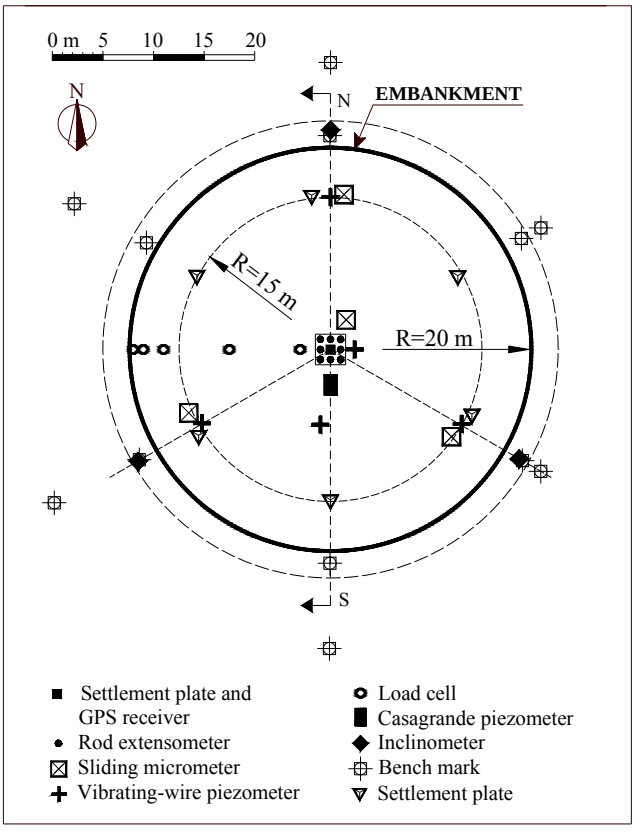

Figure 33. Embankment plan with location of monitoring devices.

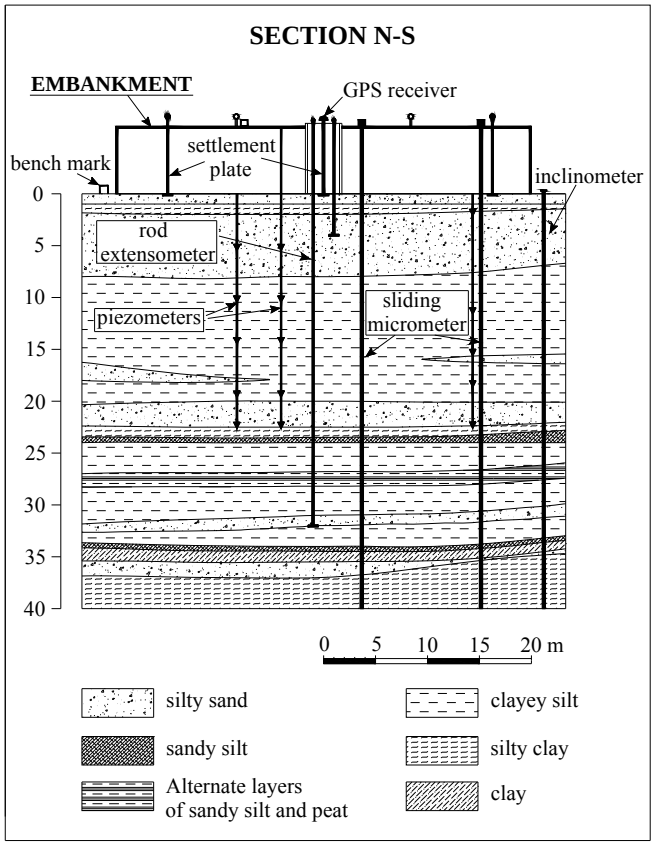

Figure 34. Cross-section of embankment with soil profile and monitoring devices.

The cylindrical sand bank construction started in September, 12th 2002 and ended in March, 10th 2003. The bank is formed by 13 geogrid-reinforced sand layers with 0.5 m thickness. The fill was a medium-fine uniform sand with D_{50}=0.14 mm. As reinforcement a stiff polypropylene geogrid was used; to avoid any sand flow through the holes of the grid, additional sheets of geotextile were placed onto the grids before placing the sand. The fill was dynamically compacted to give an average dry unit weight equal to 15.6 kN/m^3.

After completion, the embankment was covered by an impermeable membrane on which 0.2 m of medium-fine gravel was posed, thus reaching a final height of 6.7 m. Figure 35 shows the bank on completion.

Figure 35. Trial embankment on completion.

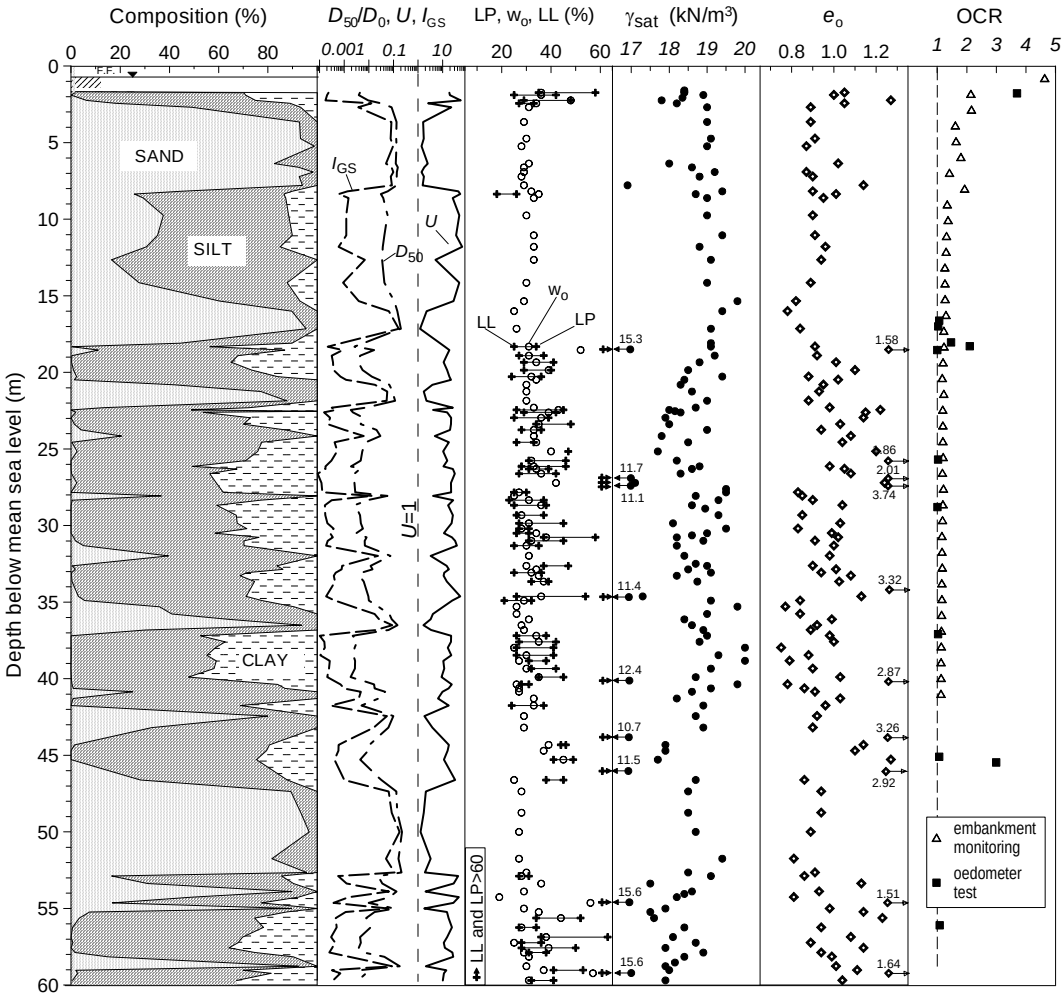

Figure 36. Soil profile, basic properties and stress history at the TTS.

4.4 *Results*

The interpretation of test data is still in progress and only some results are shown here. Staged unloading with bank removal has been planned for the end of 2006 / beginning of 2007.

4.4.1 *Soil profile, basic properties and stress history*

The approximate ground sequence, whose first 40 meters are shown on Figure 34, basically consists of:

A) 1-3 m: soft silty clay, whose drainage has been improved by prefabricated drains. This thin layer contributes significantly to the total settlement of the embankment, even though it cannot be considered as representative of the Venice lagoon cohesive formations;
B) 3-8 m: medium-fine silty sand;
C) 8-20 m: clayey silt with a sand lamination between 15 and 18 m, covering in plan a sector of 270° from North to East. This layer constitutes the fine-grained deposit that gave rise to most part of the vertical displacements;
D) 20-22 m: medium-fine silty sand;
E) 22-45 m: alternate layers of clayey and sandy silt;
F) 45-55 m: medium-fine silty sand.

Frequent laminations of peat are present below 25 m, in layers E and F.

Figure 36 reports, as a function of depth, the basic soil properties determined on laboratory samples. The profile at TTS is similar to that at MTS with the exception of the stiff OC *caranto*, which was probably here eroded during the last glaciation. This confirms the validity of the selected site to reproduce a typical Venice lagoon ground profile.

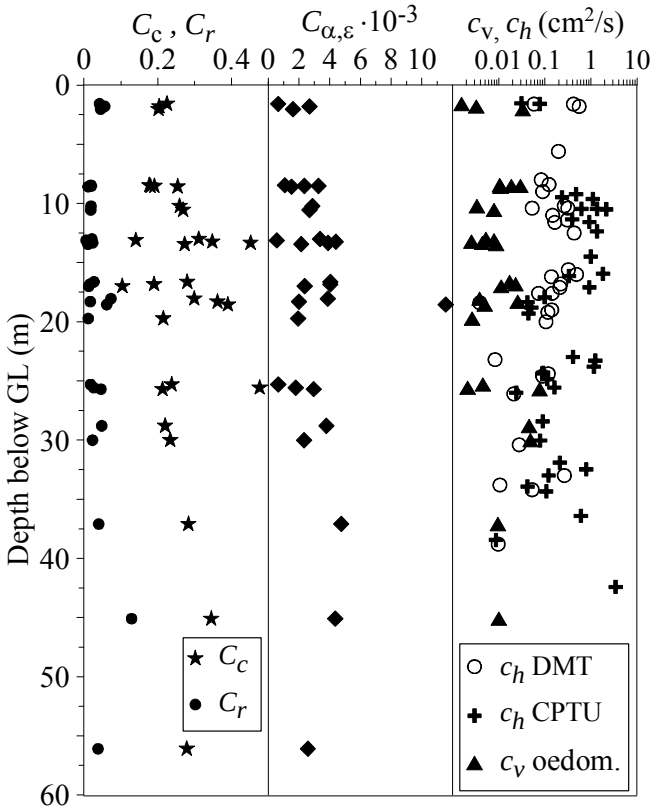

Figure 37. Profiles of compression indexes and consolidation coefficients at TTS.

Additional features to note are:

- From the soil grading reconstruction, the various types of soil occur up to 60 m, approximately, in the proportion: SM-SP 22%, ML 32%, CL 37% and CH-Pt 9%.
- Upper and deeper sands are relatively uniform; finer materials are more graded, the coarser the materials, the lower the coefficient U, with I_{GS} lying in the same range observed at MTS.
- Except for the organic soils, Atterberg limits of cohesive fraction are similar to those determined at MTS;
- The unit weight γ_{sat}, showing large oscillations with depth, is somewhat lower than that measured at MTS, void ratio e_o is slightly higher and lying approximately in the range between 0.8 – 1.1, with higher values due to laminations of organic material.

The last column of Figure 36 sketches the profile of OCR, estimated with Casagrande method on the base of oedometric test results on CL samples as well as from the interpretation of in-situ stress-strain behaviour, as described in section 4.2.4. Note that, according with in-situ response, the soil appears to be slightly overconsolidated, with a regular trend decreasing with depth. OCR estimated from oedometer tests shows a major scatter even also in specimens collected at quite the same depth, but this fact may be due to sampling disturbance and to the difficulties in applying the Casagrande method in silty materials. Other comments about OCR will be reported in section 4.2.4.

Figure 37 reports the compression and recompression coefficients C_c and C_r, the coefficient of secondary compression $C_{\alpha\varepsilon}=\Delta\varepsilon/\Delta\log(t)$ as well as the coefficients of consolidation c_v and c_h estimated from laboratory and in-situ tests. The relevant variation with depth of the coefficient of consolidation, characterized by higher c_h with respect to c_v, proves once more the relevant soil heterogeneity. To note that c_h varies in the same range measured at MTS.

The results of two typical tests CPTU14 and DMT14, carried out near the center of the embankment and at closer distance, are shown in Figure 38 in terms of profiles of significant quantities q_t, f_s, u_2, p_0, p_1 and V_s, where the latter is the shear wave velocity measured by SCPTU and SDMT.

Relevant oscillations of u_2 are clearly evident, thus suggesting large differences in drainage

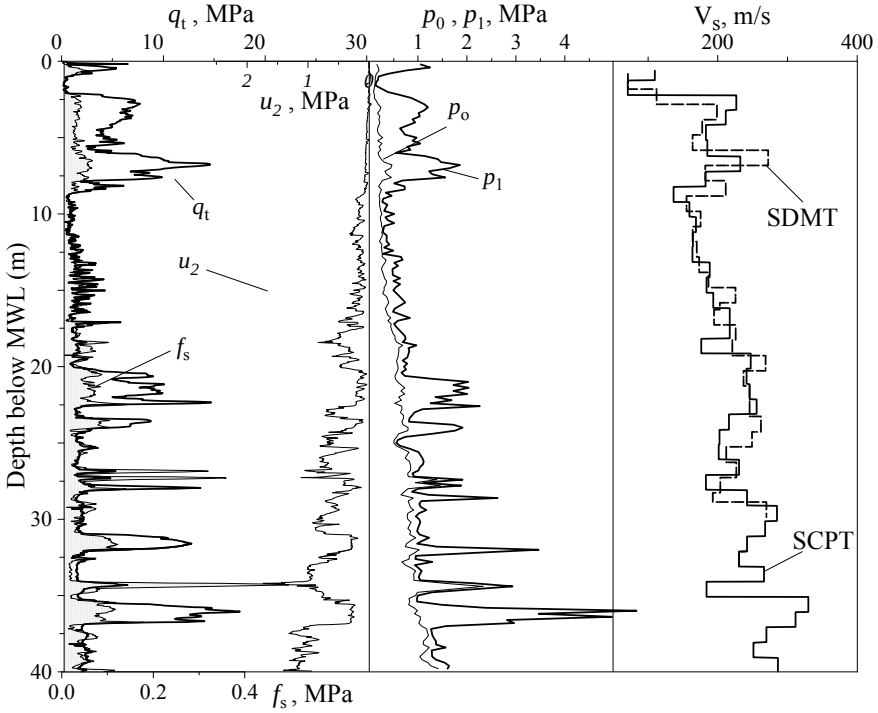

Figure 38. Comparison among the profiles of q_t, f_s, u_2, p_o, p_1 and V_s at TTS.

conditions provided by a continuous layering of different grain size composition in the whole deposit. Pore pressure parameter B_q lies in the same range measured at MTS, with some occasional values over 0.5. Similarly to MTS, V_s increases with depth from about 150 m/s to 300 m/s at higher depths.

4.4.2 *Pore pressure evolution during construction*

The presence of prefabricated drains in the upper silty clay layer A) and the relatively high soil drainage of all the deeper layers suggested that primary consolidation should have been quite rapid and contemporary with the embankment construction. In other words, no important delayed deformation due to consolidation should have been observed, considering that the rate of load increase, required by the earth-reinforcement construction technique, was low compared to the drainage conditions of the deposit.

This hypothesis seemed to be confirmed by the electric piezometer readings which gave no detectable pore pressure increase in any layer: the variation of pore pressure in the piezometers appeared to be mostly controlled by the daily oscillations of the sea tide in the channel facing the embankment area rather than by the increasing load. Casagrande piezometers measured a maximum water excursion of around 0.4 m during the whole construction interval. Figure 39 shows the results of the electric piezometer readings measured in the last loading phase together with the tide excursion measured in the canal.

4.4.3 *Vertical and horizontal displacements*

Figure 40 shows the evolution with time of the maximum ground settlement measured under the centre of the embankment. The total settlement on embankment completion (around 180 days) was 381 mm. Until the last measurement (October, 13th 2005), an additional secondary settlement at constant load of 124 mm was measured, thus giving a total settlement of 505 mm.

Figure 41 depicts the deformed ground surface at the completion of the bank and at the time of the last measurement, together with the horizontal displacements measured with one of three inclinometers. Comparing the vertical and horizontal displacements, it appeared that the total vertical displacement is one order of magnitude greater than the maximum horizontal displacement, that is, the deformation process developed prevalently in the vertical direction.

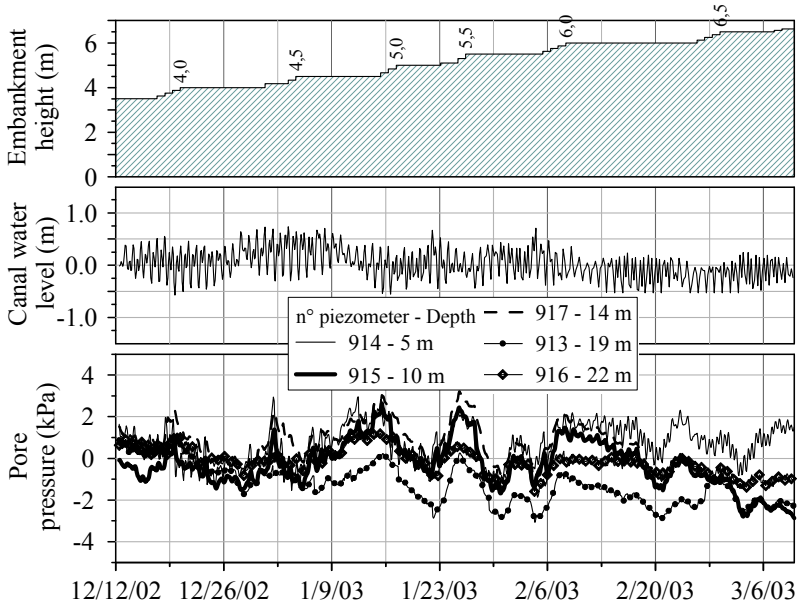

Figure 39. Pore pressure evolution during the last construction sequence.

After bank completion, a small horizontal recover seems to have probably occurred, but due to the low precision of inclinometer used for these readings this outcome cannot definitely be confirmed. The performance of GPS is also superimposed on the same plot: note the excellent agreement between the two methods of settlement measurement. GPS may be therefore an attractive alternative for a continuous vertical displacement monitoring.

It is interesting to analyze the distribution of vertical displacement with depth provided by the multiple extensometers. These measurements are given in Figures 42, both in differential and accumulated form (for the extensometer installed close to the centre).

The relevant contribution of the upper silty clay A and, particularly, of the silt layer C is clearly evident. The influence of embankment reduces with depth and beyond 35 m the

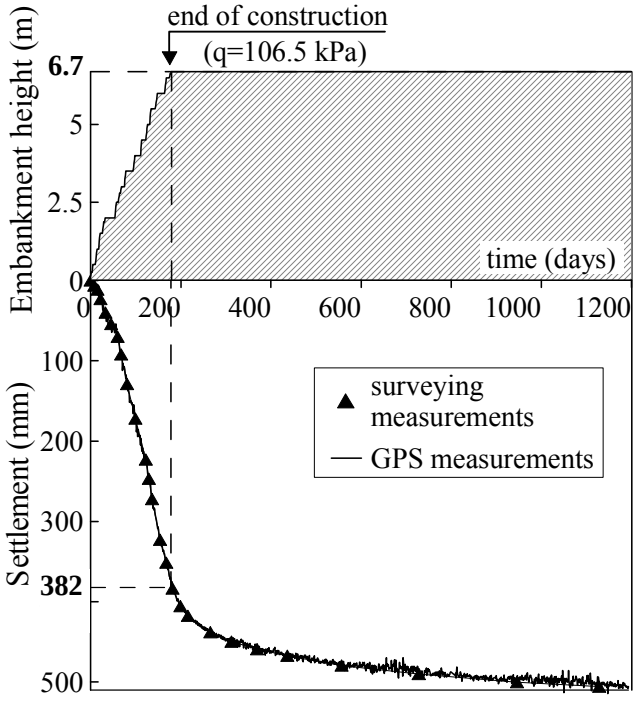

Figure 40. Evolution with time of maximum ground settlement under the embankment.

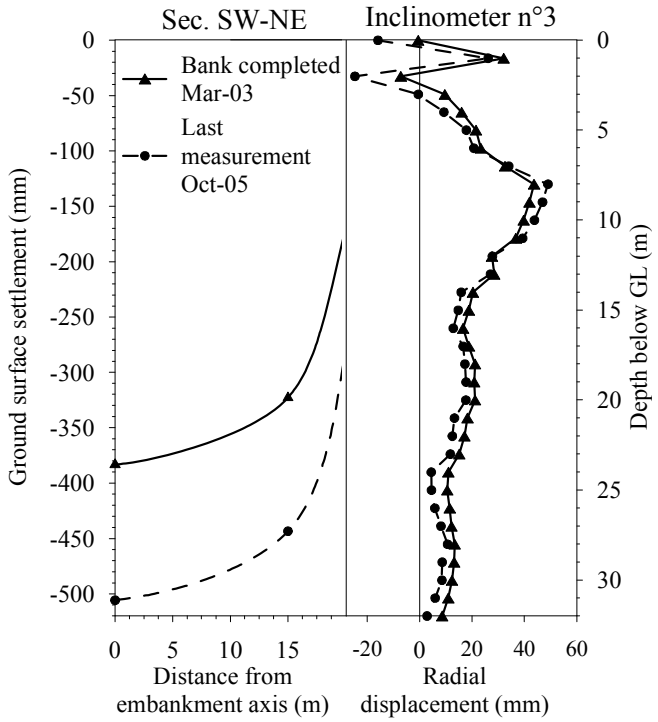

Figure 41. Vertical (centre) and horizontal (side) ground displacements.

displacements are very small and not appreciable with the type of instruments installed at TTS.

The differential displacement representation allows for an appreciation of strains, which are mostly concentrated, excluding the upper layer A, in the silty formation C. The thick continuous line marks the bank completion. Note that the maximum vertical deformation ε_z does not exceed 4% in all the layers B, C, D and E.

The vertical strain ε_z plotted as a function of increasing stress applied to the ground (the latter

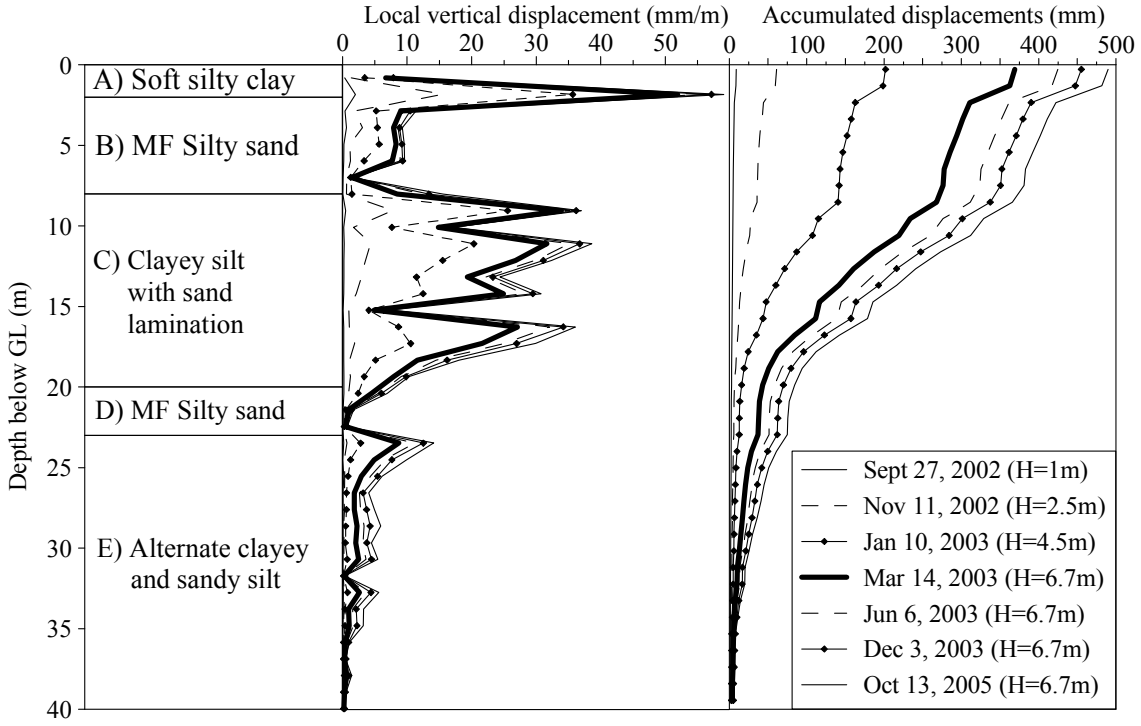

Figure 42. Local and total vertical displacements measured close to the bank centre.

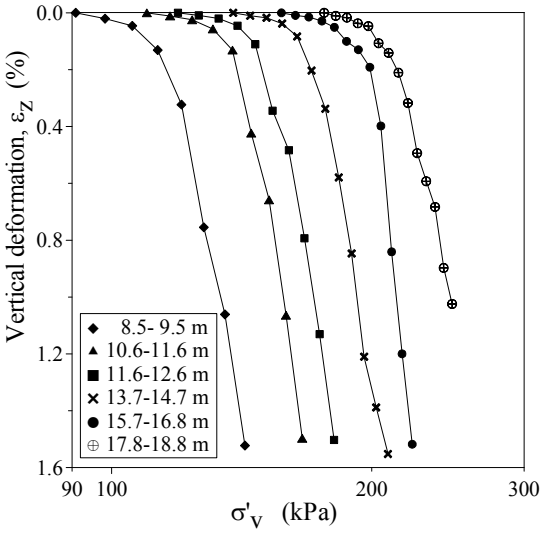

Figure 43. Vertical strain of the most compressive strata, developed during construction.

approximately estimated using an elastic finite element analysis using a realistic distribution of stiffness throughout the soil profile) allowed for a tentative evaluation of preconsolidation stress.

Figure 43 depicts a few of the typical vertical stress σ'_z vs. vertical strain ε_z responses (plotted starting from geostatic vertical effective stress σ'_{vo}) for some 1-m thick layers, recorded using the multiple extensometer located close to the bank centre. Note the variation of curvature throughout the loading process, characterized by a much stiffer response at the beginning of the loading phase.

Hypothesizing that no delayed deformation due to consolidation occurred along with the loading phase, the sharp variation of curvature was interpreted in terms of yielding stress $\sigma'_{y\text{-}site}$. Since strains in the ground developed prevalently in the vertical direction, it was tentatively assumed that the classical preconsolidation stress $\sigma'_p \approx \sigma'_{y\text{-}site}$.

Therefore, OCR calculated as $\sigma'_{y\text{-}site}/\sigma'_{vo}$ has been plotted in Figure 44. This estimate of OCR is particularly relevant, since it is the first attempt to measure directly in situ the yielding stress of Venetian materials. In addition, to better understand the origin of overconsolidation at TTS, that is erosion and/or structuration and/or delayed consolidation, the approach proposed by

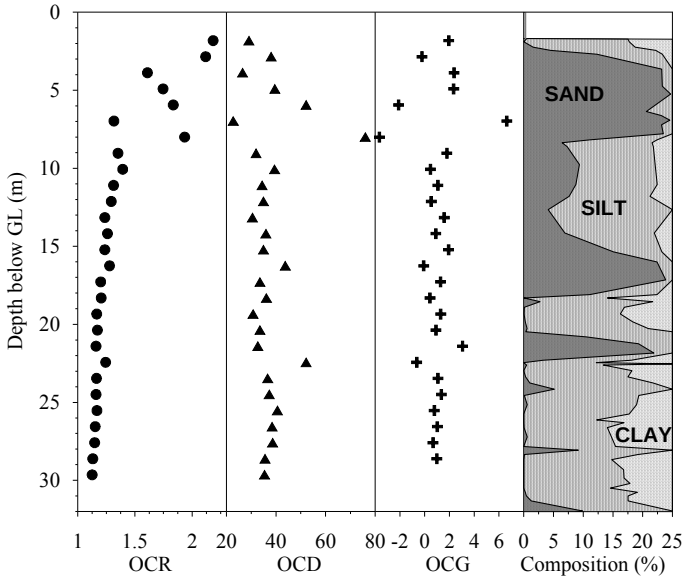

Figure 44. OCR, OCD and OCG at Treporti Test Site.

Perret et al. (1995) and discussed by Locat et al. (2003) was considered. The estimate of the overconsolidation difference OCD = σ'_p-σ'_{vo} and oveconsoildation gradient OCG = $\Delta\sigma'_p/\Delta\sigma'_{vo}$ were performed using the only available continuous OCR profile, that is, that provided by site monitoring and plotted in Figure 44. If $\sigma'_p=\sigma'_{vo}$, OCD is equal to zero and both OCR and OCD are equal to unity. Following Locat et al., a constant profile of OCD and OCG with depth means that overconsolidation is due to erosion whereas variation of one of the two quantities may be due to cementation and/or secondary compression.

The profiles plotted in Figure 44 would tentatively suggest that the small overconsolidation ratio of layers C, D and E should be mainly due to an erosion process occurred during the Pleistocene epoch rather than to cementation or secondary compression. This aspect will be further discussed in the next section.

4.4.4 *Stiffness / compressibility from site monitoring*

The high quality of measurements provided by the multiple extensometer allowed us to measure the in-situ soil stiffness, thus avoiding both the scale effect and the stress relief and/or destructuration due to sampling, particularly affecting the mechanical response of these soils.

The compression behaviour observed in the multiple extensometer located close to the bank centerline (Figure 33), whose stress-strain curves have been shown for a few of layers in Figure 43, has been interpreted in terms of:

- Initial stiffness $M_{i\text{-}site}$, evaluated as slope of the tangent to the vertical stress σ'_z vs. vertical strain ε_z curves;
- Tangent stiffness $M_{site} = \Delta\sigma'_z/\Delta\varepsilon_z$ evaluated for each loading step;
- Compression index CR_{site} defined as slope of ε_z-logσ'_z curves beyond estimated yielding stress $\sigma'_{y\text{-}site}$;
- Secondary compression index $C_{\alpha\varepsilon\text{-}site}$ defined as slope of the ε_z-log(time) curves after the end of embankment construction.

The initial stiffness $M_{i\text{-}site}$ representing the maximum site stiffness, is plotted against depth in Figure 45. For sake of comparison, the trend of maximum stiffness, evaluated with the down-hole seismic piezocone and converted into elastic modulus (for elastic isotropic medium) in both confined (M_{SCPTU}) and unconfined conditions (E_{SCPTU}) using a Poisson ratio = 0.20, is also depicted in Figure 46. As expected, $M_{i\text{-}site}$ is characterized by values lower than the SCPTU

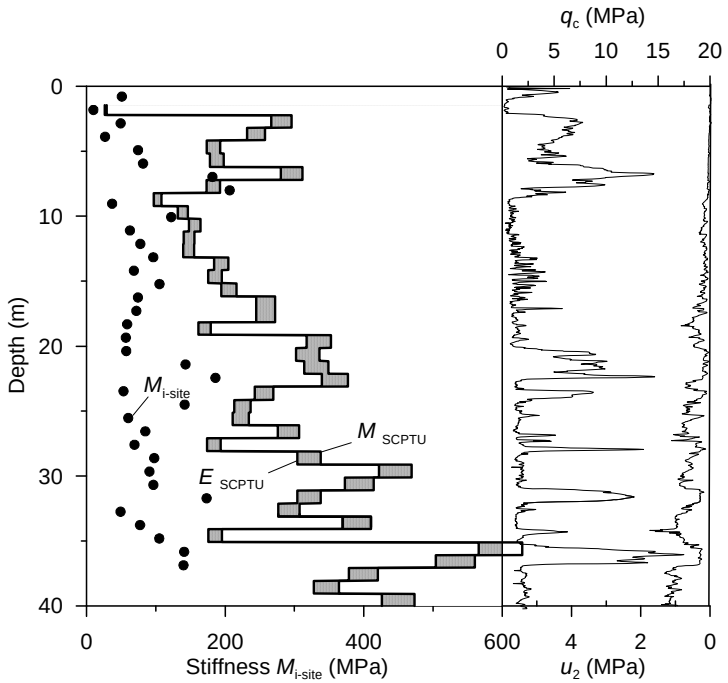

Figure 45. Comparison between initial stiffness and maximum stiffness from SCPT test.

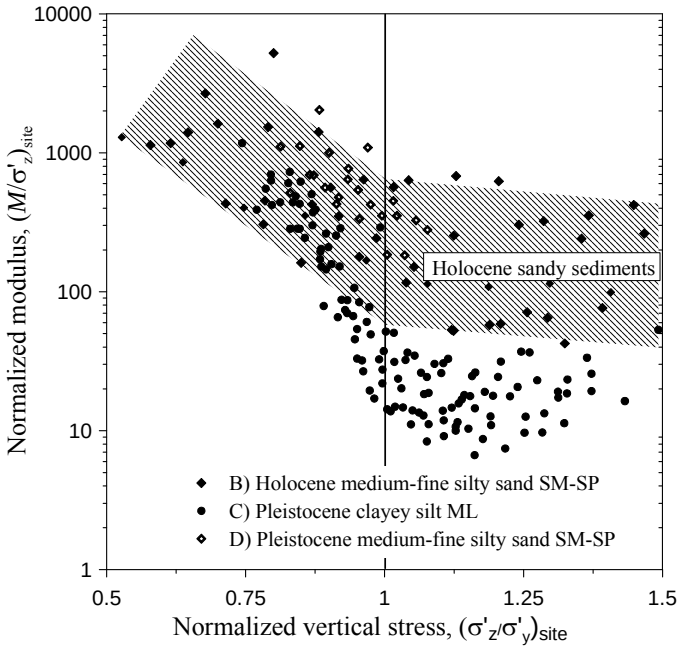

Figure 46. Normalized tangent stiffness vs. normalized vertical stress.

stiffness profile, except a few of shallower layers where $M_{i\text{-site}}$ seems to approach the SCPTU stiffness.

Normalized modulus $(M/\sigma'_z)_{site}$ of layers B, C and D is plotted in Figure 46 against normalized current vertical stress $(\sigma'_z/\sigma'_y)_{site}$ induced by the increasing embankment load. Note the sharp variation of $(M/\sigma'_z)_{site}$ trends for clayey silts of layer C before and after the yield stress, that clearly separates the behaviour in OC from NC range. Both Holocene and Pleistocene sands are clearly characterized by higher values, whose variation is less influenced by the overcoming of the in-situ yield stress.

Assuming tentatively that the deformation process under the bank centerline approaches the 1-D condition, the $(M/\sigma'_z)_{site}$ values of the thick silty layer B is compared in Figure 47 with the

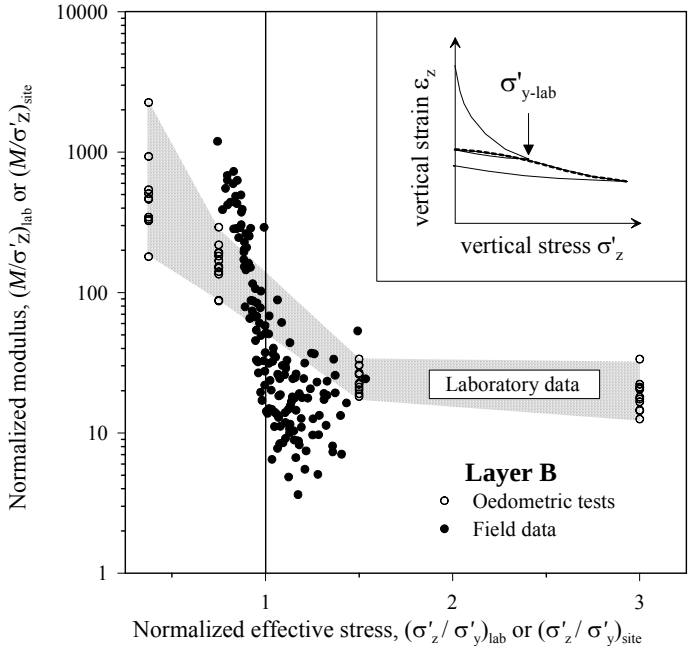

Figure 47. Site and laboratory normalized tangent stiffness vs. normalized vertical stress.

laboratory values of the normalized constrained modulus $(M/\sigma'_z)_{lab}$ obtained from one-dimensional compression tests. In order to compare data as homogeneous as possible, $(M/\sigma'_z)_{lab}$ was calculated through the interpretation of the recompression curve in an unloading-reloading cycle followed by the virgin compression part (dashed line shown in the upper-right part of Figure 47). With this procedure, the normalizing yielding stress is the maximum vertical stress before an unloading-reloading cycle, that is, the precompression effect on the response in 1-D tests is due only to mechanical imposed precompression, thus reducing possible intrinsic influence of ageing or secondary compression or structuration on soil stiffness.

It is important to notice that field data cross the laboratory trend: the stiffness before yielding stress is significantly higher compared to laboratory data whereas beyond $(\sigma'_z/\sigma'_y)_{lab}$ it reduces to significantly lower values. This may be tentatively explained considering the effect of disturbance and stress relief due to sampling that removes from laboratory material response any influence of ageing / secondary compression / structuration. From the above considerations, it seems that the small precompression observed in Pleistocene formations at TTS should be probably due to the combined effect of mechanical precompression and ageing, not excluding the possible influence of a very small structuration.

The slope of the site compression curves, whose typical trend is depicted in Figure 43, was interpreted (after overcoming the yield stress) in terms of virgin compression coefficient CR_{site} and plotted in Figure 48 as a function of depth. Values of CR_{lab}, defined like the ratio $\Delta\varepsilon_z/\Delta\log(\sigma'_z)$ after yielding in 1-D compression tests, are superimposed on the same graph. Note that CR_{lab} was estimated, as commonly done in current engineering practice, in a range of vertical effective stress well above that induced in situ by the embankment loading.

Figure 49 shows typical ε_z vs. log(time) curves evaluated for each 1-m thick layer. The strain-time trend is characterized by a *S-type* shape with the final part, corresponding to deformation occurring after bank construction, fitted in the ε_z-log*t* plane by a straight line whose slope is assumed to be the site secondary compression coefficient $C_{\alpha\varepsilon\text{-site}} = \Delta\varepsilon_z/\Delta\log t$. A comparison with laboratory $C_{\alpha\varepsilon-lab}$ is tentatively proposed for the layers B, C and D, assuming, again, that the site deformation process under bank centreline approaches the 1D response. The comparison is carried out in Figure 50 in terms of Mesri's approach considering the ratio between primary and secondary compression $(C_{\alpha\varepsilon}/CR)_{site}$. As found at MTS, upper $(C_{\alpha\varepsilon}/CR)_{site}$ values are due to SM-SP material, intermediate to CL and lower to ML. However no appreciable difference is noticed among the three different soil classes. $(C_{\alpha\varepsilon}/CR)_{site}$ ratios are similar to those from the laboratory,

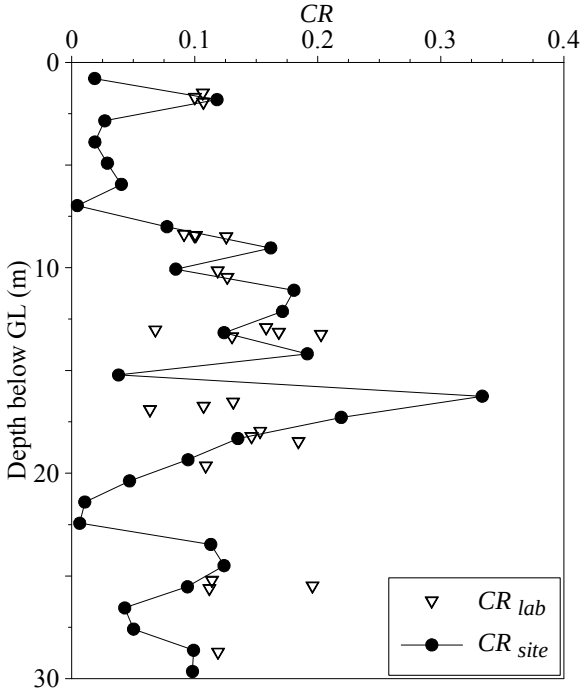

Figure 48. Site and laboratory virgin compression coefficients.

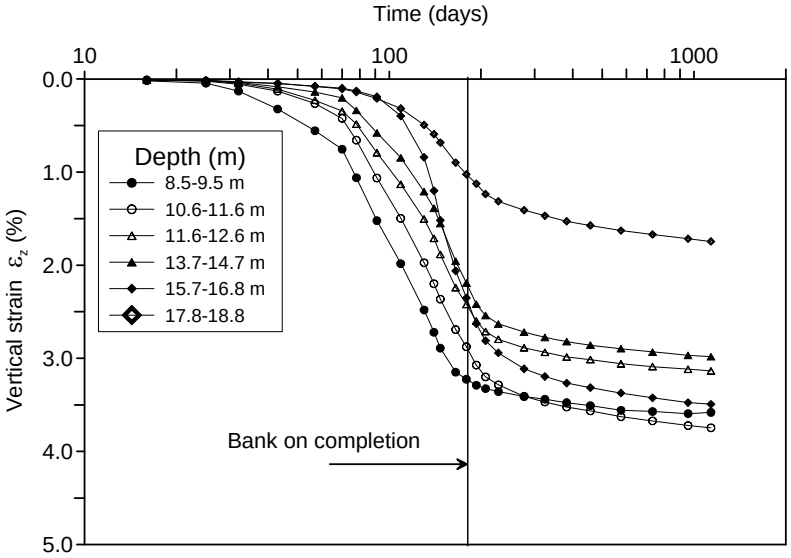

Figure 49. Typical trends of vertical strain vs. time measured with the multiple extensometer.

but with upper values due to the deep formation E, (composed prevalently of silty clay and clayey silt with some important peat lamination) and lower values for the upper formation C (composed of sandy silts). $(C_{\alpha\varepsilon}/CR)_{site}$ for sandy layer of formation B is somewhat external to the typical range suggested by Mesri.

5 CONCLUSIONS

The paper outlined some relevant results of the research carried out so far to characterize the mechanical behavior of Venice lagoon heterogeneous silts.

The information obtained from the investigation carried out at the Malamocco Test Site is now being improved by a new experimental study at the Treporti Test Site, whose results, based on the directly in-situ measurement of the stress-strain-time soil properties, appear to represent a unique and valuable tool for a suitable calibration of CPTU and DMT and for the formulation of a reliable geotechnical model aimed at an appropriate design of the mobile gate foundations.

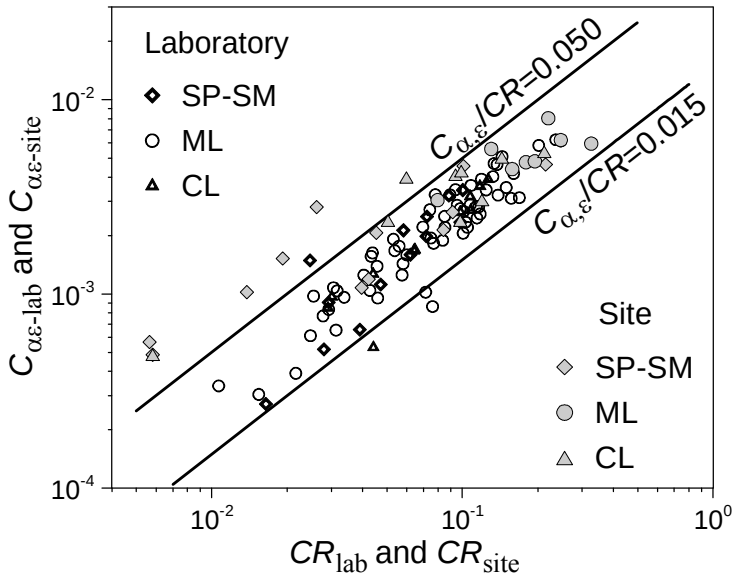

Figure 50. Site and laboratory primary and secondary compression coefficients.

AKNOWLEDGEMENTS

The authors wish to extend special thanks to: the Consorzio Venezia Nuova, the Magistrato alle Acque, the research groups of the University of Bologna and of L'Aquila; Prof. P.W. Mayne of GeorgiaTech, USA; everybody at the geotechnical group of the University of Padova.

REFERENCES

Baldi, G., Bellotti, R., Ghionna, V.N., Jamiolkowski, M. & Lo Presti, D.C.F. 1989. Modulus of Sands from CPT and DMT. *XII ICSMFE*, Rio de Janeiro, Vol. 1, pp. 165-170, Rotterdam: Balkema.

Been, K., Jefferies, M.G. & Hachey, J. 1991. The critical state of sands. *Géotechnique,* 41(3): 365-381.

Been, K. & Jefferies, M.G. 1985. A state parameter for sands. *Géotechnique*, 35(2): 91-112.

Bolton, M.D. 1986. The strength and dilatancy of sands. *Géotechnique,* 36(1): 65-78.

Bolton, M.D. 1987. Discussion. *Géotechnique*, 37(2): 225-226.

Biscontin, G., Pestana, J., Cola, S. & Simonini, P. 2001. Influence of grain size on the compressibility of Venice Lagoon soils. *XV ICSMGE*, Istanbul, Vol.1, pp. 35-38, Rotterdam: Balkema.

Biscontin, G., Pestana, J., Cola, S. & Simonini, P. 2006. A unified compression model for the Venice lagoon natural silts. *J. of Geotechnical and Geoenvironmental Eng., ASCE*, submitted.

Bonatti E. 1968. Late-Pleistocene and Postglacial Stratigraphy of a Sediment Core from the Lagoon of Venice (Italy). *Mem. Biog. Adr.*, Venezia, Vol. VII (Suppl.), pp. 9-26.

Butterfield, R., Gottardi, G., Simonini, P. & Cola, S. 2003. A new interpretation of the compressibility of Venetian silty-clay soils. *BGA International Conference on Foundations, Innovations, Observations, Design and Practice*, Vol. 1, pp. 149-159, Thomas Telford, London, UK.

Cola, S. 1994. Caratterizzazione geotecnica delle argille di Fusina. PhD Thesis, University of Padova. (*in italian*)

Cola, S. & Simonini, P. 1999. Some remarks on the behavior of Venetian silts, *2nd Int. Symp. on Pre-failure behaviour of geomaterials*, IS Torino 99, pp. 167-174, Rotterdam: Balkema.

Cola, S & Simonini, P. 2002. Mechanical behaviour of silty soils of the Venice lagoon as a function of their grading properties. *Canadian Geotechnical J.*, 39(4): 879-893.

Colombo, P. 1986. La difesa di Venezia dai fiumi e dal mare. *Rivista Italiana di Geotecnica*, 20, 73-92.

Colombo, P. & Matteotti, G. 1967. Caratteristiche geotecniche di alcuni terreni tipici dei bacini di Malamocco e Chioggia nella laguna di Venezia. *Atti dell'Istituto Veneto di Scienze, Lettere ed Arti.* Tomo CXXV, 312-323. (*in italian*)

Cortellazzo, G., Bellis, G., Dalla Vedova, B., Ramigni, M. & Simonini, P. 1995. Soil properties by computed tomography and needle probe method. *Proc. 11th ECSMFE, Copenhagen*, Danish Geotechnical Society, Copenhagen.

Curzi, P.V. 1995. *Sedimentological-environmental study of the Malamocco inlet: Final report.* Consorzio Venezia Nuova, Venezia.

Department of Earth Sciences of University of Ferrara 2004. Analisi della carota CH1T prelevata a Bocca di Lido (Venezia). *Rapporto Finale*. (In Italian)

Dobry, R. & Vucetic M. 1987. Dynamic properties and seismic response of soft clay deposits. *Int. Symp. on Geotech. Eng. of Soft Soils.* Vol. 2, Soc. Mex. Mech. Suelos.

Durgunoglu, H.T. & Mitchell, J.K. 1975. Static penetration resistance of soils: I. Analysis. *Proc. ASCE, Specialty Conference on In Situ Measurements of Soil Properties*, Raleigh, NC, Vol.1, pp. 151-172.

Favero V., Alberotanza L. & Serandrei Barbero R. 1973. Aspetti paleoecologici, sedimentologici e geochimici dei sedimenti attraversati dal pozzo VE1bis. *CNR, Laboratorio per lo studio della dinamica delle grandi masse, Rapporto tecnico n.63*, Venezia. (*in italian*)

Gatto P. & Previatello P. 1974. Significato stratigrafico, comportamento meccanico e distribuzione nella Laguna di Venezia di un'argilla sovraconsolidata nota come "Caranto". *CNR, Laboratorio per lo studio della dinamica delle grandi masse, Rapporto tecnico n.70*, Venezia. (*in italian*)

Gentilomo, M. 1997. The Venice lagoon project. Mobile barriers at the lagoon inlets for controlling high tides. *Symposium "Venice and Florence. A complex dialogue with water.",* ITCOLD, Italian Committee for Large Dams, May 24th. Florence, 31-53, Patron, Bologna.

Gottardi, G. & Tonni, L. 2004. A comparative study of piezocone tests on the silty soils of the Venice lagoon (Treporti Test Site). *ISC-2, Geotechnical and Geophysical Site Characterization*, Porto, Vol. 2, pp. 1643-1649, Rotterdam: Millpress.

Graham, J. & Houlsby, G.T. 1983. Anistropic elasticity of a natural clay. *Géotechnique*, 33(2): 165-180.

Grozic, J.L.H., Lunne, T. & Pande, S. 2003. An oedometer test study on the preconsolidation stress of glaciomarine clays. *Canadian Geotechnical J.*, 40: 857-872.

Hardin, B.O. & Black, W.L. 1969. Vibration modulus of normally consolidated clay. *J. of SMFE Div., Proc. ASCE*, 95(SM1): 33-65.
Hardin, B.O. & Drnevich, V.P. 1972. Shear modulus and damping in soils: design equations and curves. *J. of SMFE Div., Proc. ASCE*, 98(SM7): 667-692.
Harleman, D.R.F., Bras, R.L., Rinaldo, A. & Malanotte, P. 2000. Blocking the Tide, *Civil Enginering, ASCE*: 52-57.
Hegazy, Y. A. & Mayne, P.W. 1995. Statistical correlation between V_s and cone penetration data for different soil types. *Int. Symposium on Penetration Testing*, *CPT '95*, Linkoeping, Vol. 2, pp.173-178, Swedish Geotechnical Society.
Hryciw, R.D. 1990. Small-strain-shear modulus of soil by dilatometer. *Journal of Geotechnical Engineering*, ASCE, 116(11): 1700-1716.
Ishihara, K., Tatsuoka, F., & Yashuda, S. 1975. Undrained strength and deformation of sand under cyclic stresses. *Soils and Foundations*, 15(1): 29-44.
Jamiolkowski, M., Ghionna, V.N., Lancellotta, R. & Pasqualini, E. 1988. New correlations of penetration tests for design practice, *Penetration Testing 88, ISOPT-1*, pp. 263-296, Balkema, Rotterdam.
Janbu, N. 1963. Soil compressibility as determined by oedometer and triaxial tests. *Proc. 3rd ECSMFE*, Wiesbaden, Vol. 1, pp. 245-251.
Kovari, K. & Amstad, C. 1982. A new method of measuring deformations in diaphragm walls and piles. *Geotéchnique*, 22(4): 402-406.
Lacasse, S. & Lunne, T. 1988. Calibration of dilatometer correlations, *Penetration Testing 88, ISOPT-1*, pp. 539-548, Rotterdam: Balkema.
Lee, K.L. & Seed, H.B. 1967. Drained strength characteristics of sands. *J. Soil Mech. Found. Div., ASCE*, 99(SM6): 117-141.
Leroueil, S. & Hight, D.W. 2002. Behaviour and properties of natural soils and soft rocks. *Overview paper. Characterization and Engineering Properties of Natural Soils*, Vol. 1, pp. 29-254, Tan et al. eds., Swets and Zeitlinger, The Netherlands.
Locat. J., Tanaka, H., Tan, T.S., Dasari, G.R. & Lee, H. 2003. Natural soils: Geotechnical Behaviour and Geological knowledge. *Overview paper. Characterization and Engineering Properties of Natural Soils*, Vol. 1, pp. 3-28, Tan et al. eds., Swets and Zeitlinger, The Netherlands.
Marchetti, S. 1975. A new in-situ test for the measurement of horizontal soil deformability. *Proc. Am. Soc. Civ. Engrs. Spec. Conf. In-situ measurements of soil properties*, Vol. 2, pp. 255-259.
Marchetti, S. 1980. In situ tests by flat dilatometer, *J. of Geot. Eng., ASCE*, 106(GT3): 299-321.
Marchetti, S. & Crapps, D.K. 1981. Flat Dilatomer Manual, *Schmertmann and Crapps*, Inc. Gainsville.
Marchetti, S., Monaco, P., Calabrese, M. & Totani, G. 2004. DMT- predicted vs. measured settlements under a full-scale instrumented embankment at Treporti (Venice), Italy. *ISC'02*, *Geotechnical and Geophysical Site Characterization*, Porto, Vol. 2, pp. 1511-1518, Rotterdam: Millpress.
Mayne, P.W. 1991. Determination of OCR in clays by piezocone tests using cavity expansion and critical state concepts, *Soils and Foundations*, 31(2): 65-76.
Mayne, P.W. & Rix, G.J. 1993. G_{max}-q_c relationships for clays. *Geotechnical Testing Journal*, 16(1): 54-60.
Mayne, P. & McGillivray, A. 2004. Seismic piezocone and seismic flat dilatometer tests at Treporti. *Proc. ISC'02*, *Geotechnical and Geophysical Site Characterization*, Porto, Vol. 2, pp. 1695-1701, Rotterdam: Millpress.
Mesri, G. & Godlewski, P. M. 1977. Time- and stress- compressibility relationship. *JGED*, ASCE, 105(GT5): 417-430.
Mesri, G., Shahien, M. & Feng, T.W. 1995. Compressibility parameters during primary consolidation. *Proc. Int. Symp. On Compression and Consolidation of Clayey Soils – IS Hirishima '95*, Hiroshima, 2, pp. 1021-1037.
Olsen, R.S. & Farr, J.V. 1986. Site characterization using the Cone Penetrometer Test, *Proc. Int. Symp. IN-SITU '86,* Blacksburg (USA), pp. 854-868.
Perret, D., Locat, J. & Leroueil, S. 1995. Strength development with burial in fine-grained sediments from the Saguenary Fjord, Quebec. *Canadian Geotechnical J.*, 32: 247-262.
Powers, M.C. 1953. A new roundness scale for sedimentary particles. *J. Sedim. Petrol*., 23: 117-119.
Randolph, M.F. 2004. Characterization of soft sediments for offshore applications. Keynote lecture. Proc. *ISC'02*, *Geotechnical and Geophysical Site Characterization*, Porto, Vol. 1, pp. 209-232, Millpress. Rotterdam.
Ricceri, G. & Butterfield, R. 1974. An analysis of compressibility data from a deep borehole in Venice, *Geotechnique*, **24** (2), 175-192.
Ricceri, G., Simonini, P. & Cola, S. 2002. Applicability of piezocone and dilatometer to characterize the soils of the Venice lagoon. *Geotechnical and Geological Engineering*, 20(2): 89-121.
Robertson, P.K. & Campanella, R.G. 1983. Interpretation of cone penetration test, Part I: Sands. *Canadian Geotechnical J.*, 20(4): 718-734.

Robertson, P. K. 1990. Soil classification using the cone penetration test, *Canadian Geotechnical J.*, 27: 151-158.

Rowe, P.W. 1973. Soil mechanic aspect of the cores of the deep borehole VE 1 in Venice. A critical analysis and recommended future investigations. *Technical Report N. 57. National Research Council*, Venice.

Senneset, K., Janbu, N. & Svano, G. 1982. Strength and deformation parameters from cone penetration tests. *Proc. 2nd Eur. Symp. on Penetration Testing*, Amsterdam, Vol. 2, pp. 863-870, Rotterdam: Balkema.

Simonini P. & Cola S. 2000. Use of piezocone to predict maximum stiffness of Venetian soils. *Journal of Geotechnical and Geoenvironmental Engineering*, *ASCE*, 126(4): 378-381.

Simonini, P. 2004. Characterization of the Venice lagoon silts from in-situ tests and the performance of a test embankment. Keynote Lecture. *Proc. ISC'02*, *Geotechnical and Geophysical Site Characterization.* Porto, 1, pp. 187-207, Rotterdam: Millpress.

Tatsuoka, F. & Ishihara, K. 1974. Drained deformation of sand under cyclic stress reversing direction. *Soils and Foundations*, 14(3): 51-65.

Tatsuoka, F. & Shibuya, S. 1992. Deformation characteristics of soils and rocks from field and laboratory tests. *Report of the Institute of Industrial Science of the University of Tokyo*.

Torstensson, B.A. 1975. Pore pressure sounding instrument. *Proc. Spec. Conf. In-situ measurements of soil properties*, *ASCE,* Vol. 2, pp. 48-54.

Torstensson, B.A. 1977. The pore pressure probe. *Nordiske Geoteknisk Mote*, Oslo, Paper N. 34.

Totani, G., Marchetti, S., Monaco, P. & Calabrese, M. 1999. Impiego della prova dilatometrica (DMT. nella progettazione geotecnica. *XX National Geotechnical Congress*, Parma, Italy, Vol. 1: 301-308.

Wood, D., Belkeir, K. & Liu, D.F. 1994. Strain softening and state parameter for sand modelling. *Géotechnique*, 44(2): 335-339.

Wroth, C.P. & Bassett, R.H. 1965. A stress-strain relationship for the shearing behaviour of sand, *Géotechnique*, 15(1): 32-56.

Wroth, C.P. 1984. The interpretation of in situ soil tests. *Géotechnique*, 34(4): 449-489.

Yu, H. S. & Mitchell, J. K. 1998. Analysis of cone resistance: review of methods. *J. of Geotechnical and Geoenviromental Engineering*, ASCE, 124(2): 140-149.